

Cosmic rays at the knee

Results and implications



«ETTORE MAJORANA» FOUNDATION AND CENTRE FOR SCIENTIFIC CULTURE

INTERNATIONAL SCHOOL OF COSMIC-RAY ASTROPHYSICS
«MAURICE M. SHAPIRO»

23rd Course: "Multi-Messenger Astroparticle Physics" 20 – 28 July 2024

PRESIDENT AND DIRECTOR OF THE CENTRE: PROFESSOR A. ZICHICHI

DIRECTORS OF THE COURSE: PROFESSORS J.R. HÖRANDEL, T. STANEV, R. SPARVOLI - J.P. WEFEL (director emeritus)



Nikhef



Jörg R. Hörandel

RU Nijmegen, Nikhef, VU Brussel

<http://particle.astro.ru.nl>

Cosmic rays at the knee

Results and implications

energy density

$$\rho_E = \frac{4\pi}{c} \int \frac{E}{\beta} \frac{dN}{dE} dE \approx 1 \frac{\text{eV}}{\text{cm}^3}$$

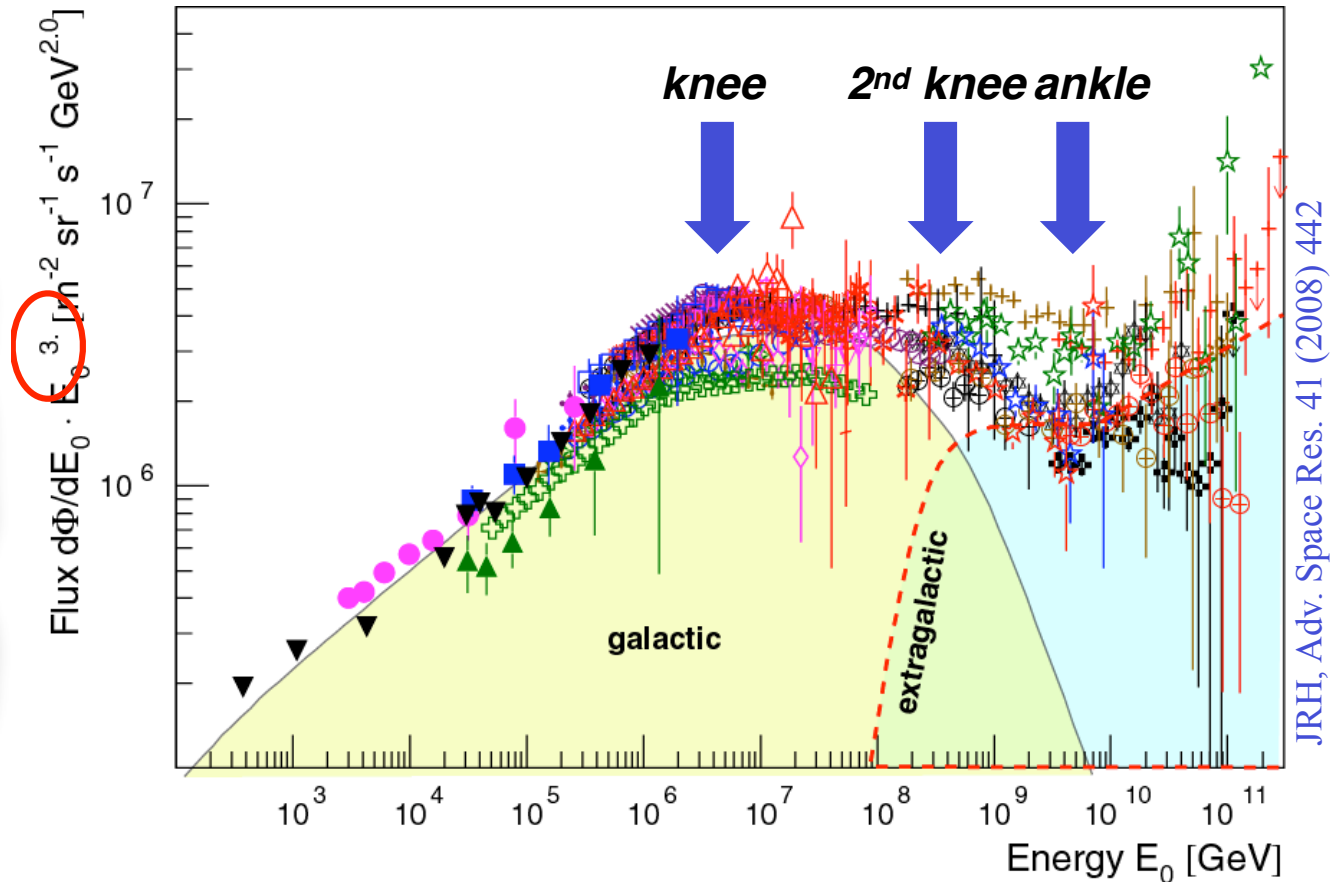
for comparison:

$$\rho_B = \frac{B^2}{2\mu_0} \approx 0.25 \text{ eV/cm}^3$$

$$\rho_{SL} \approx 0.3 \text{ eV/cm}^3$$

$$\rho_{IR} \approx 0.4 \text{ eV/cm}^3$$

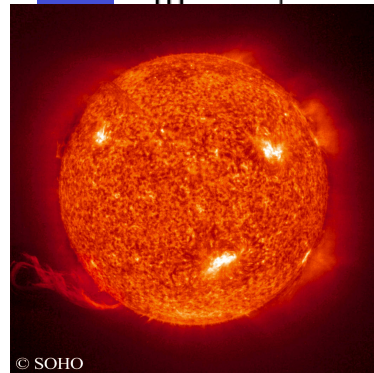
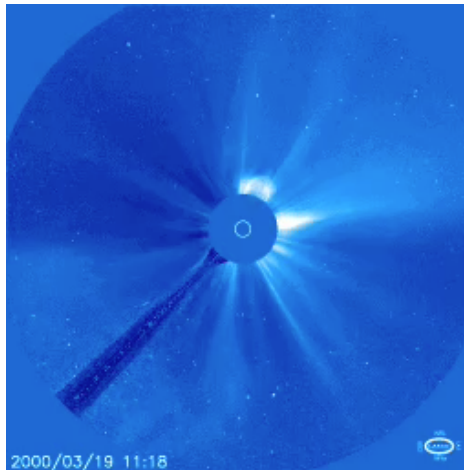
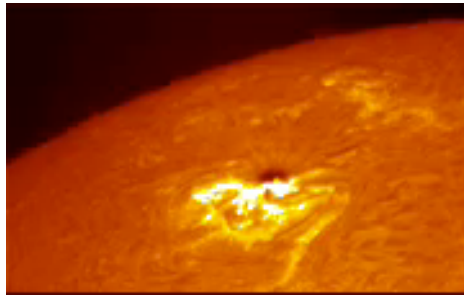
$$\rho_{3K} \approx 0.25 \text{ eV/cm}^3$$



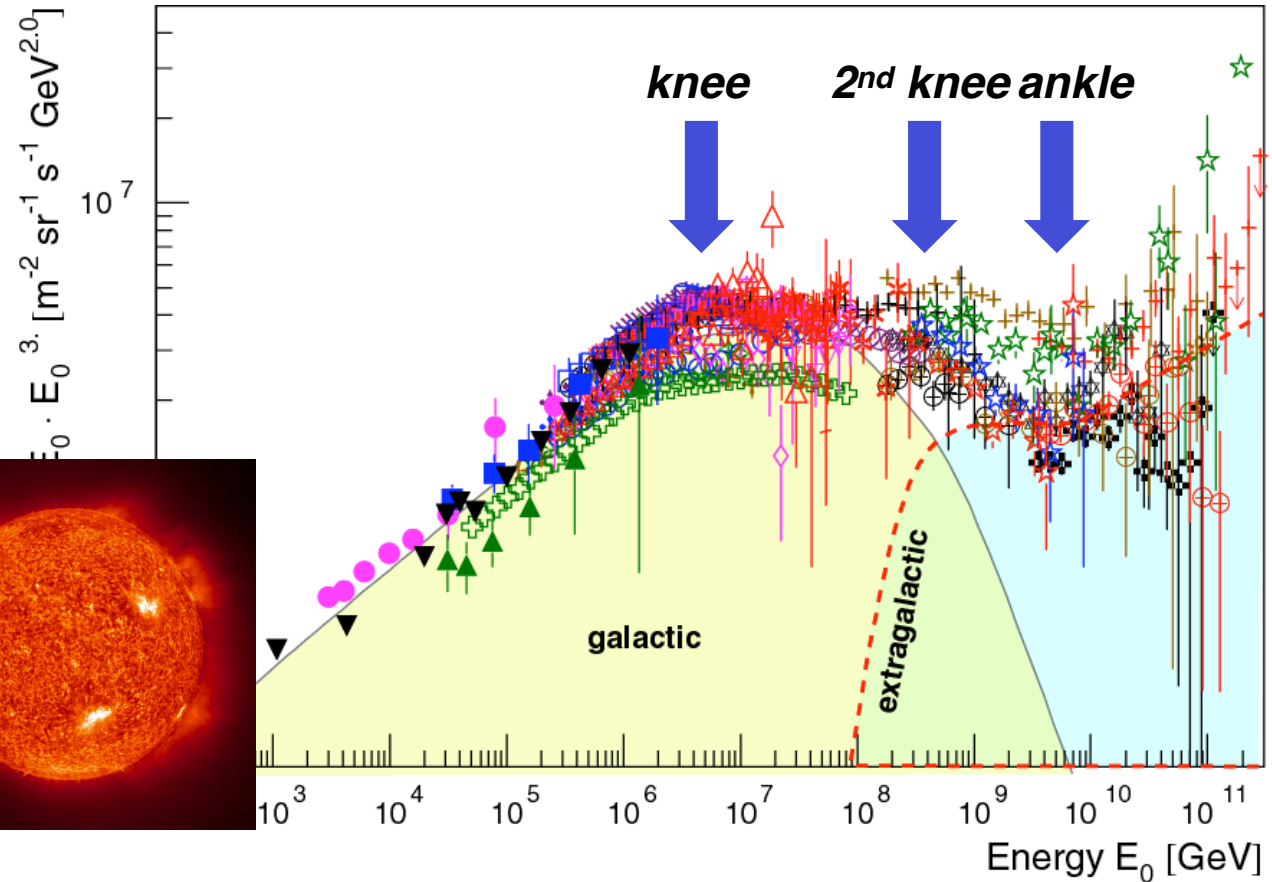
Cosmic rays at the knee

Results and implications

Solar flares



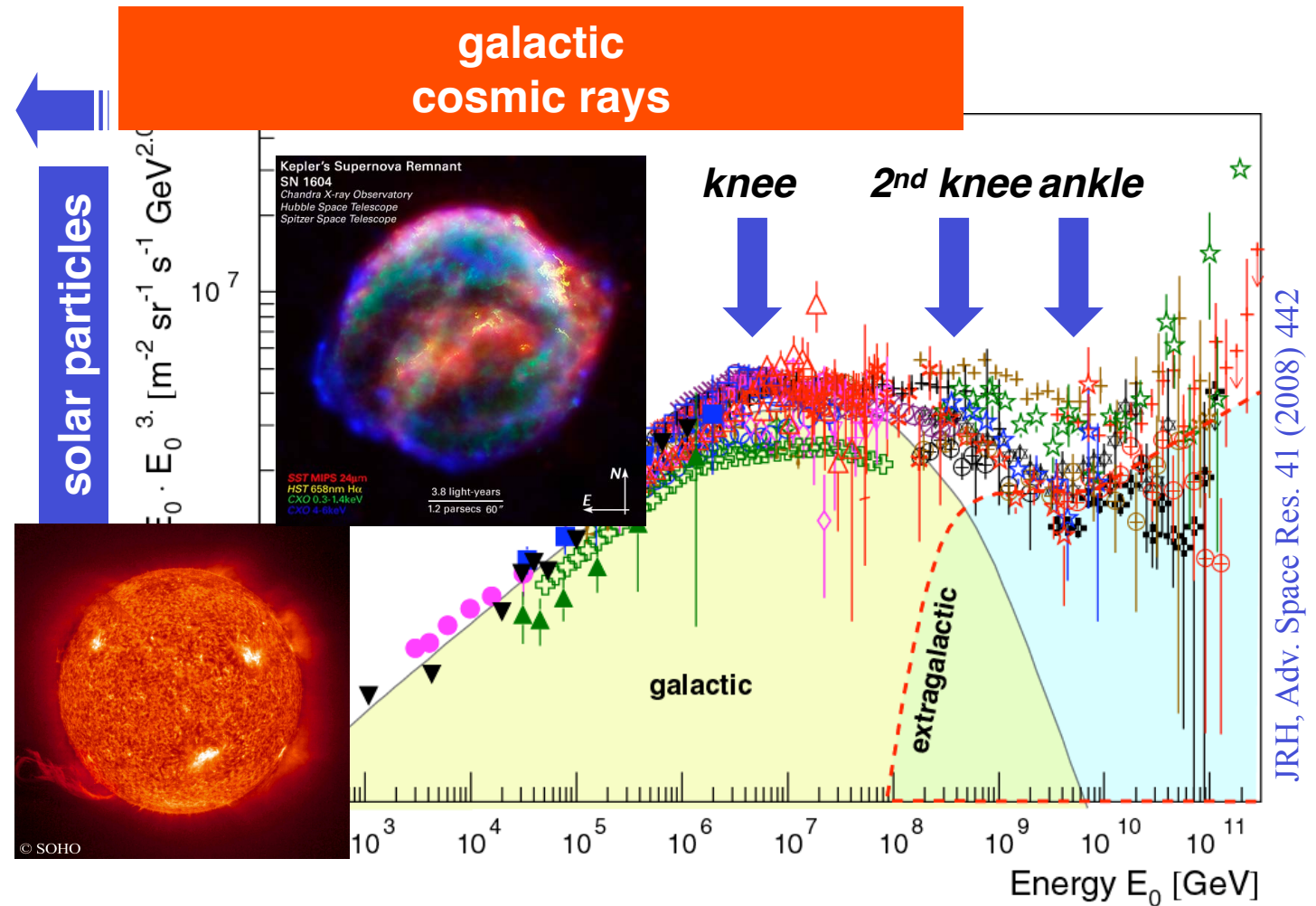
solar particles



JRH, Adv. Space Res. 41 (2008) 442

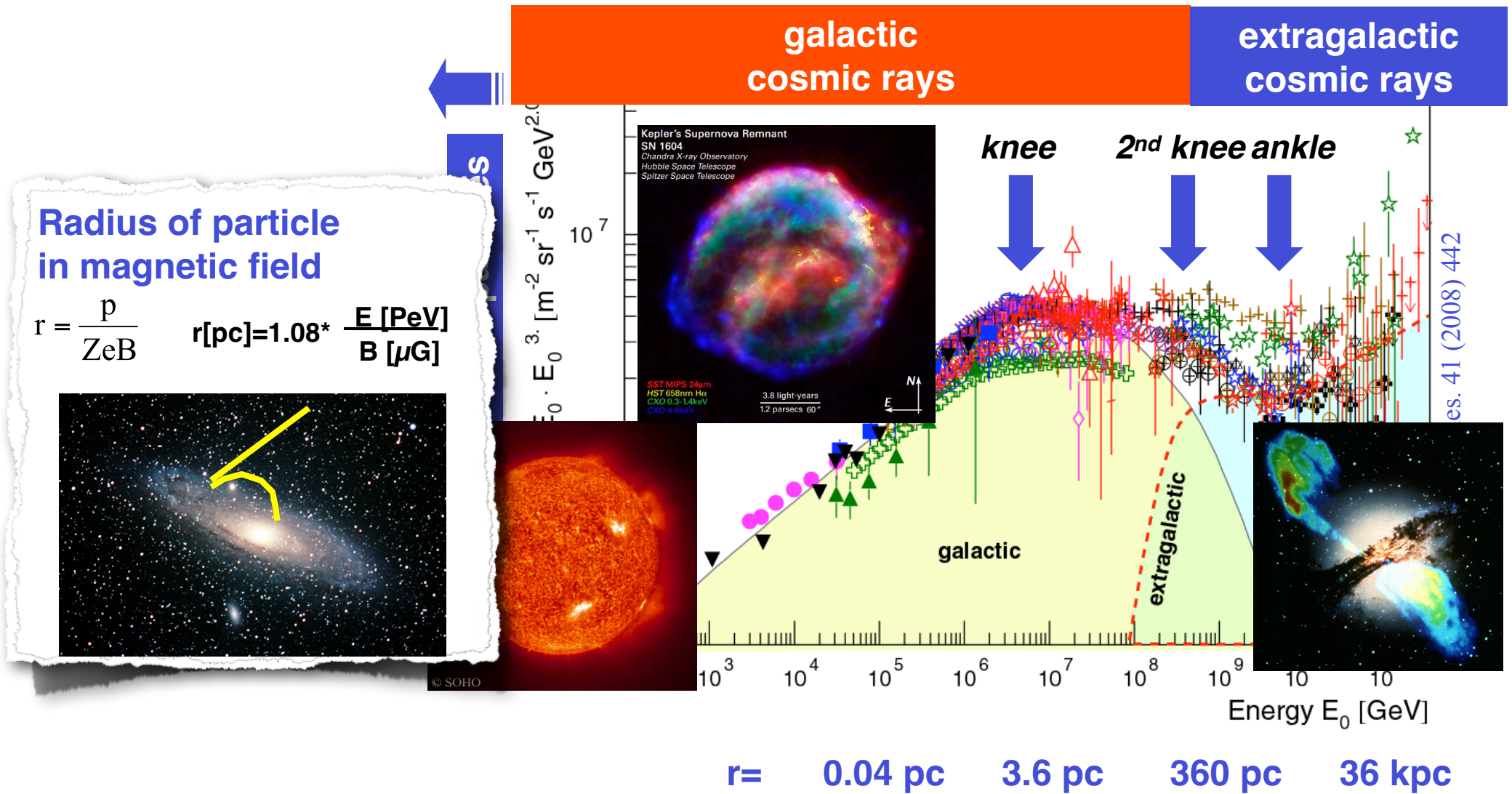
Cosmic rays at the knee

Results and implications



Cosmic rays at the knee

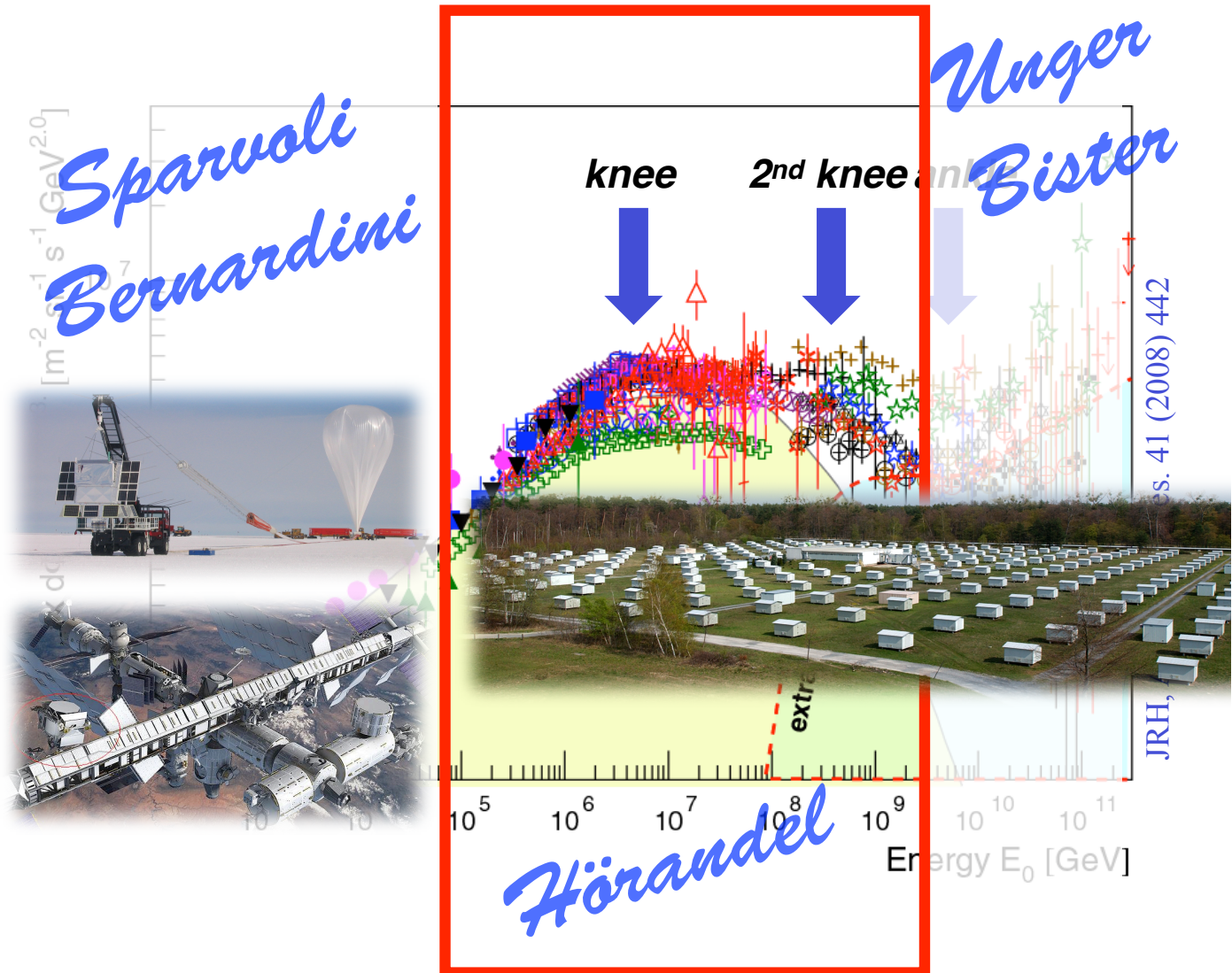
Results and implications



Cosmic rays at the knee

galactic
cosmic rays

extragalactic
cosmic rays



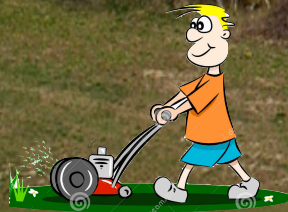
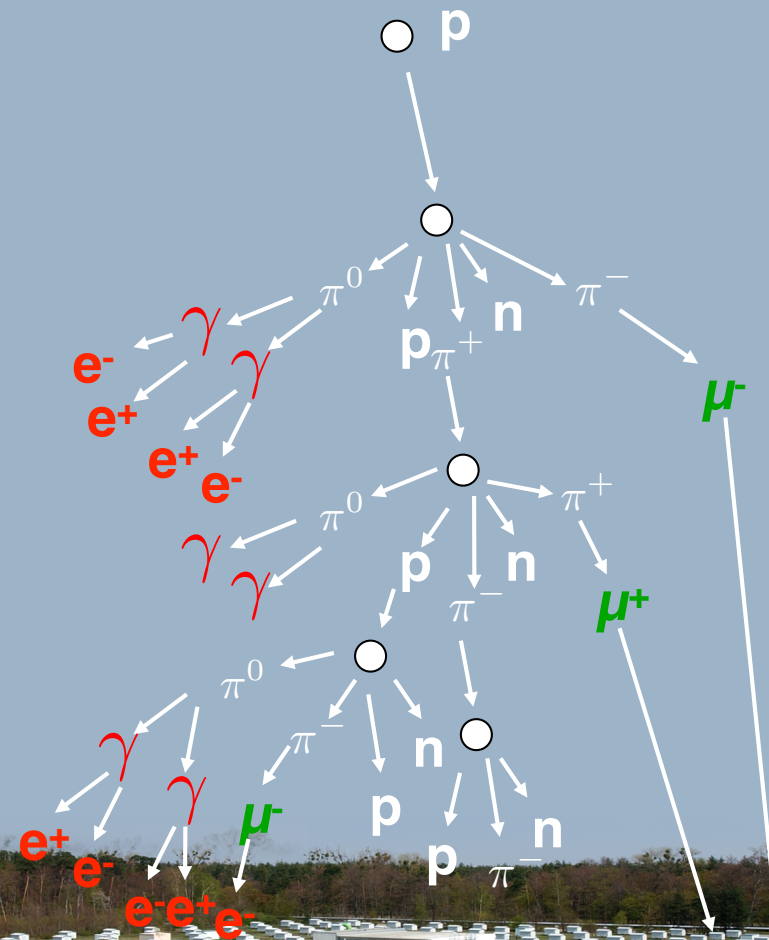
Extensive Air Showers

electromagnetic hadronic **muonic**
shower component

~ 98%

< 1%

~2%



A Matthews Heitler Model – mass resolution in EAS measurements

depth of shower maximum

$$X_{\max}^A = X_{\max}^p - X_0 \ln A$$

radiation length $X_0=36.7 \text{ g/cm}^2$

typical uncertainty

$$\Delta X_{\max} \approx 20 \text{ g/cm}^2$$

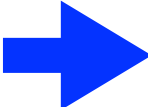
expected mass resolution


$$\Delta \ln A \approx 0.8 - 1$$

electron-muon ratio

$$\lg(N_e/N_\mu) = C - 0.065 \ln A.$$

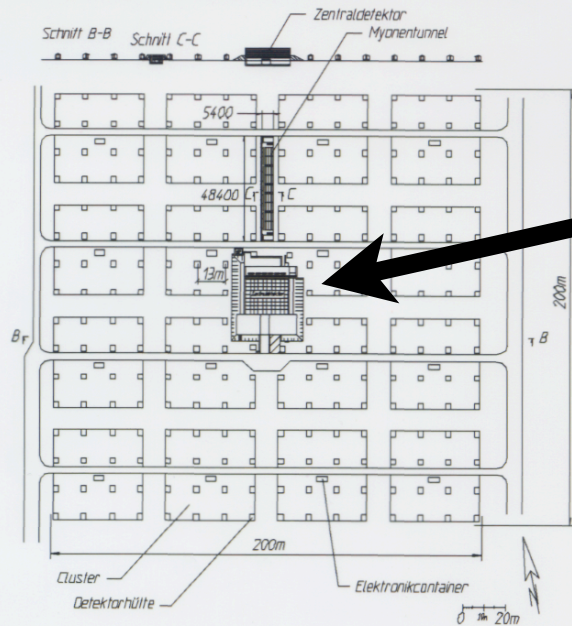
$$\Delta \frac{N_e}{N_\mu} \approx 16\% - 20\%$$



**4 to 5 mass groups
p, He, CNO, (Si), Fe**

The KASCADE Array

200 m



Array

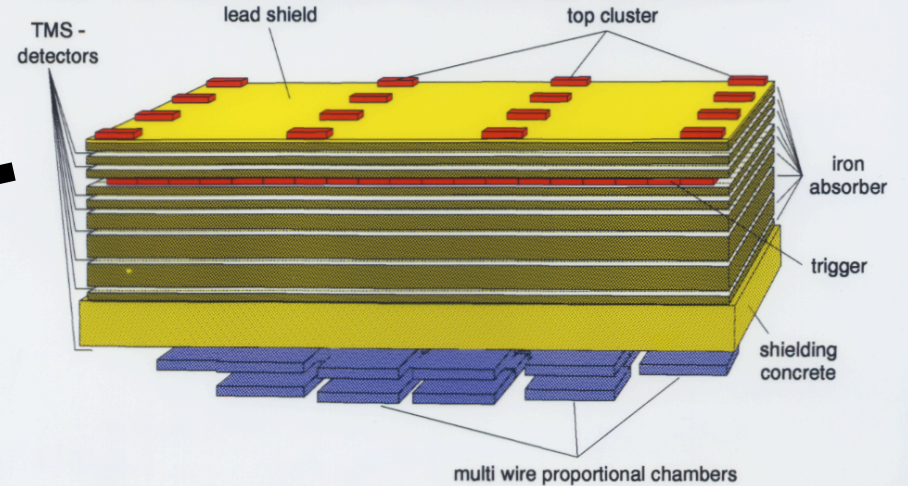
200 m

252 stations with

- e/γ detectors: 4 cm liquid scintillator ($\approx 3.1 \text{ m}^2$)
- muon detectors: 3 cm plastic scintillator ($\approx 3.2 \text{ m}^2$)
- shield 10 cm Pb + 4 cm Fe $\rightarrow 20 X_0$
- ⇒ $E_\mu > 300 \text{ MeV}$
- measurement of particle densities and arrival times

JRH 06/96

The KASCADE Central Detector



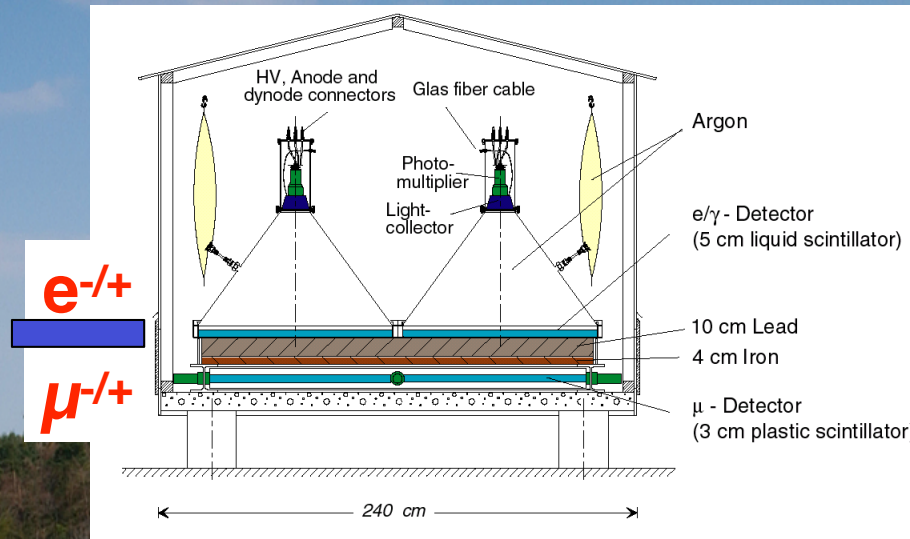
4 different detector systems:

- Top array $32 \times 0.45 \text{ m}^2$ scintillation counters (14 m^2)
- Trigger layer $456 \times 0.45 \text{ m}^2$ scintillation counters (206 m^2)
- 32 Multiwire proportional chambers ($2 \times 150 \text{ m}^2$) $E_\mu > 2 \text{ GeV}$
- Iron sampling calorimeter ($16 \times 20 \text{ m}^2$)
- 8 active layers $\rightarrow 10\,000$ liquid ionisation chambers
- 40 000 electronic channels
- separation of individual hadrons by a fine segmentation
- depth $\approx 11 \lambda_i \rightarrow$ hadrons up to 10 TeV 95% contained

JRH 06/96

KARlsruhe Shower Core and Array DEtector

Simultaneous measurement of
electromagnetic,
muonic,
hadronic
shower components

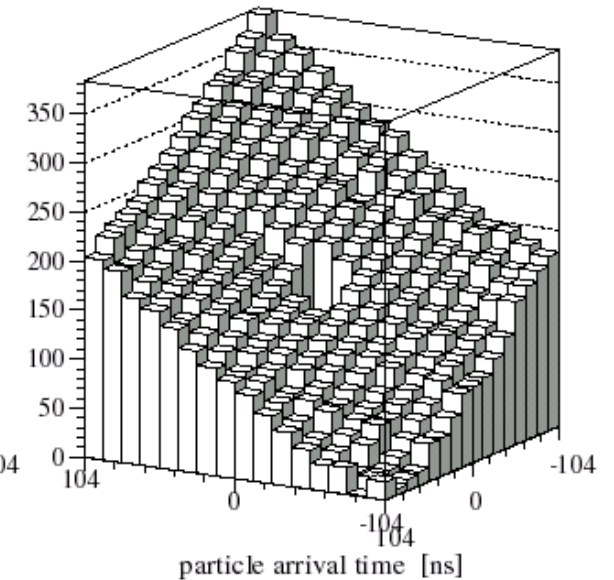
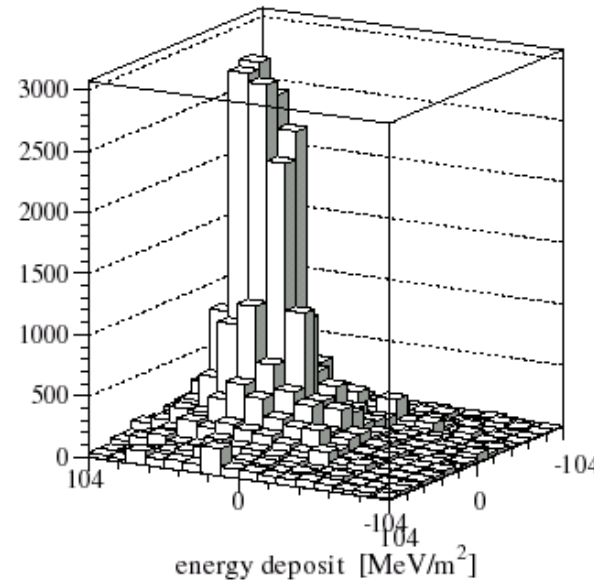
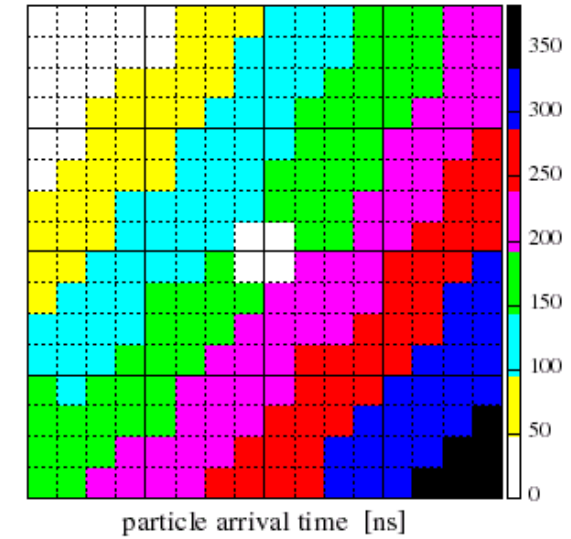
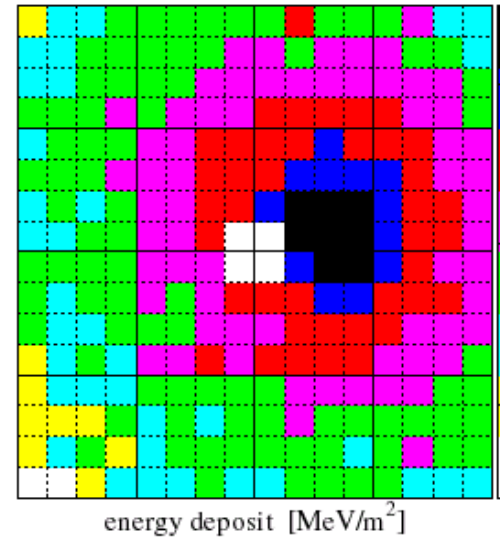


Event reconstruction in the scintillator array

electromagnetic component

e/ γ -Detectors, Run 1, Event 71089, 96-03-05 22:07:48.956078

shower core	$\Delta r = 2.5 - 5.5 \text{ m}$
shower direction	$\Delta \alpha = 0.5^\circ - 1.2^\circ$
shower size	$\Delta N_e/N_e = 6 - 12 \%$



KASCADE GRANDE Array

37 detector stations

370 m² e/ γ :
scintillation counter



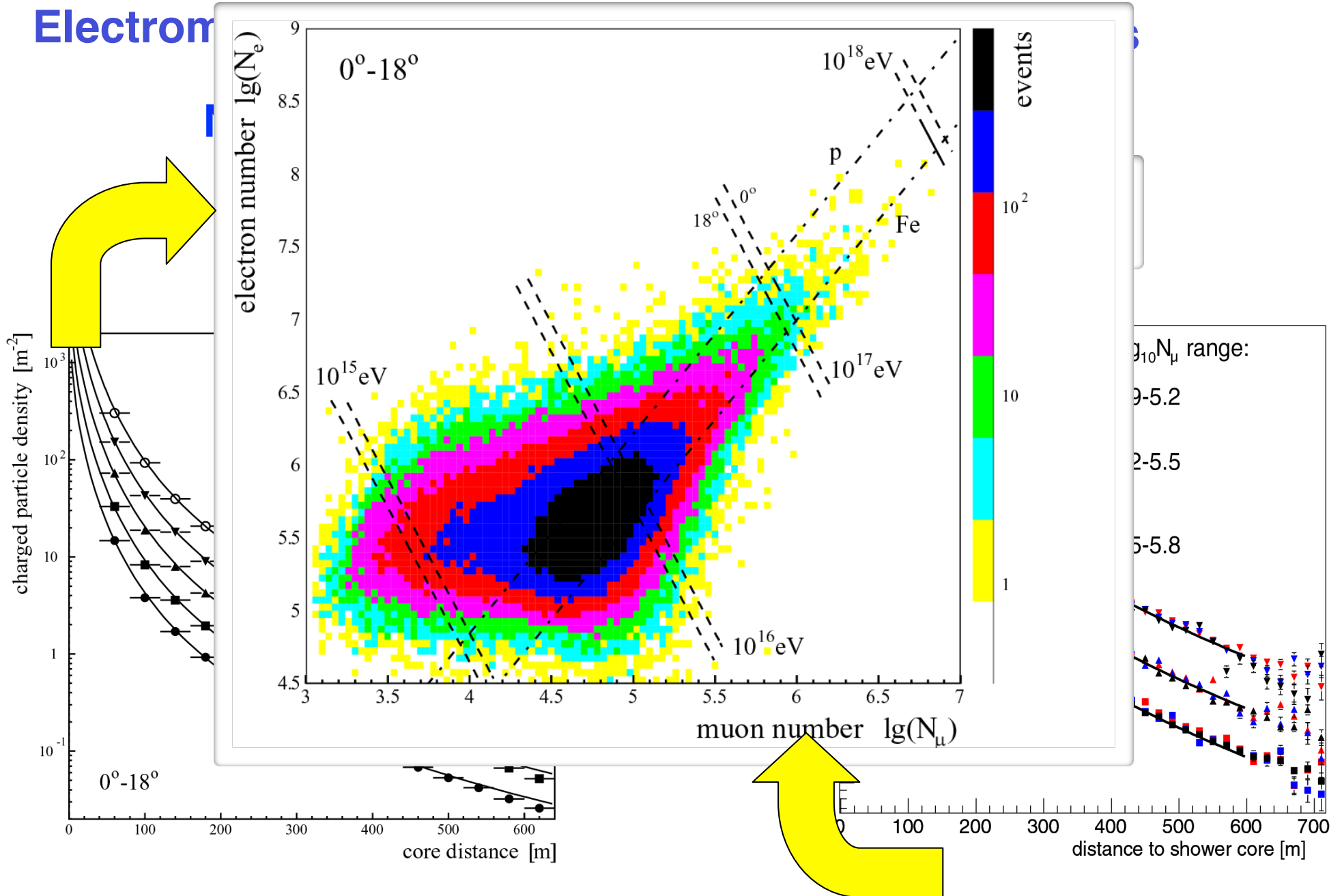
KASCADE

200 m x 200 m

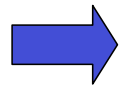
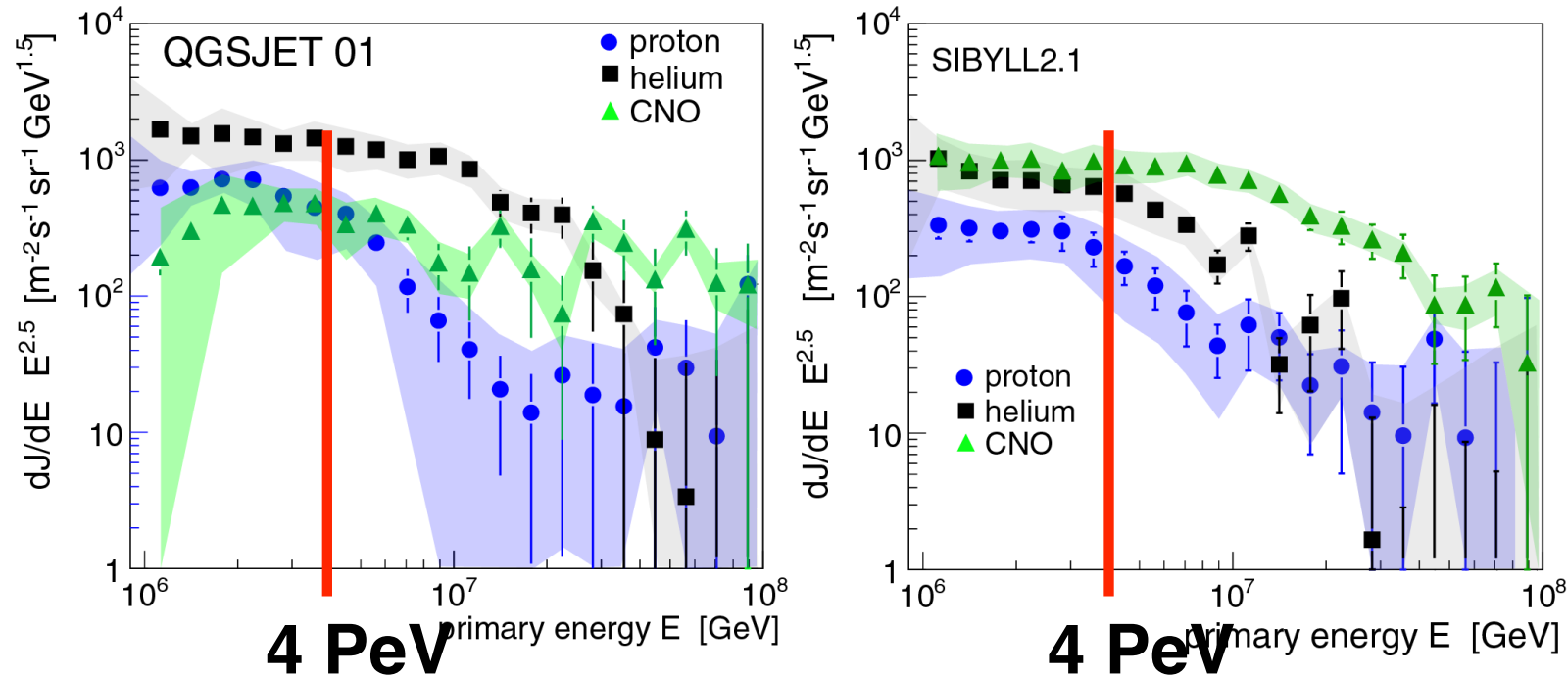
700 m

700 m

KASCADE-Grande – Lateral distributions



KASCADE: Energy spectra for elemental groups



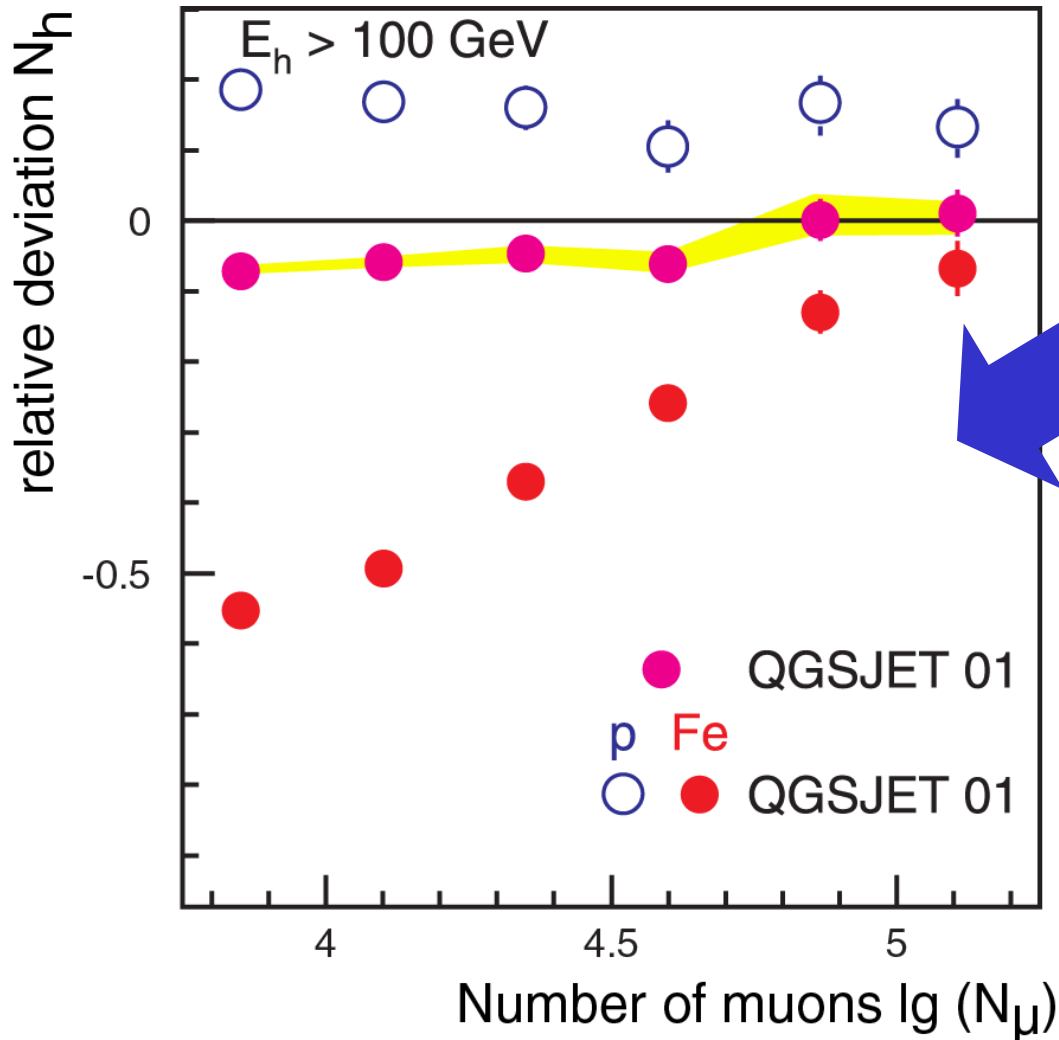
Knee caused by cut-off for light elements

**Astrophysical interpretation
limited by description of
interactions in the atmosphere**

Test of hadronic interaction models

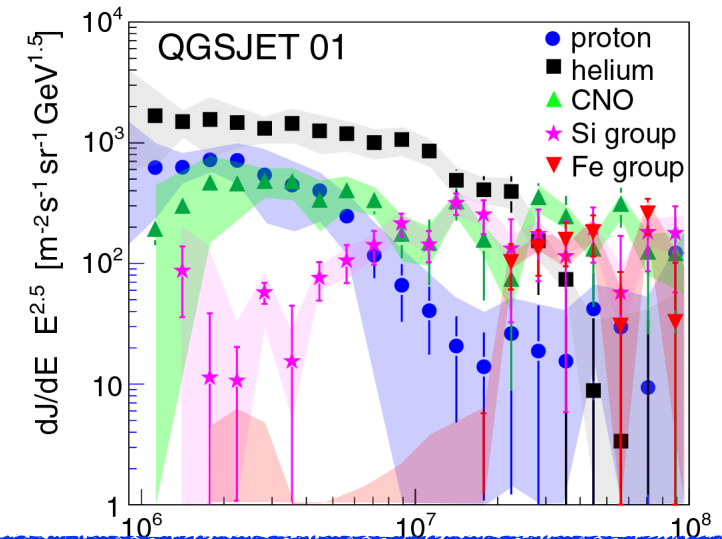
QGSJET 01

Number of hadrons vs. number of muons



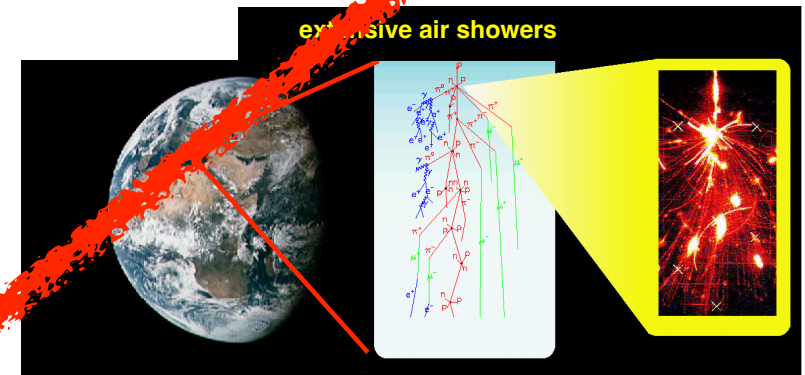
inconsistencies on 10% level

N_e - N_μ analysis



in literature:

**ideas that knee is caused by new interactions in atmosphere
 —> energy is carried away by „invisible channels“**



Electron, muon and hadron size spectra of EAS in the "knee" region
R. Glasstetter^a and J.R. Hörandel^a for the KASCADE Collaboration^a

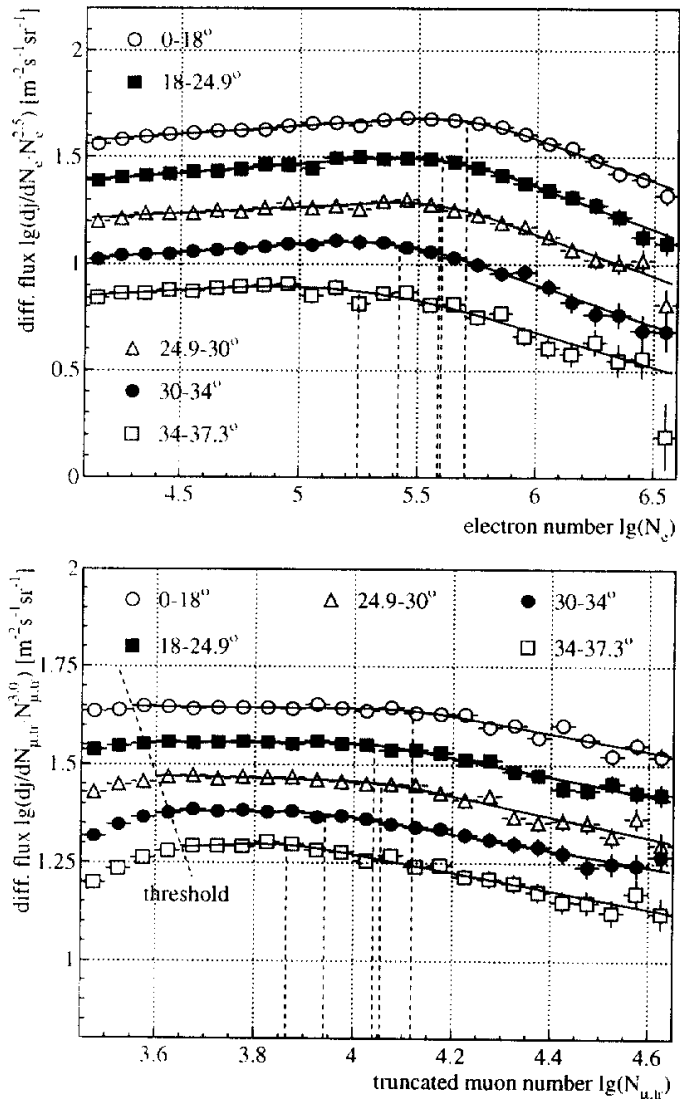


Figure 1. Electromagnetic (top) and muonic (bottom) shower size spectra for different zenith angle bins.

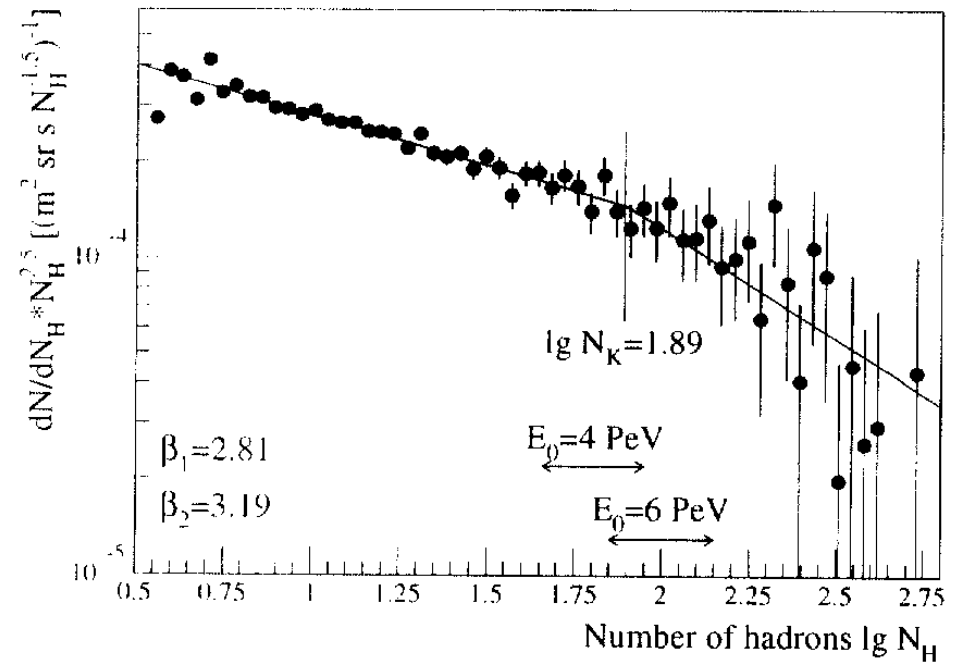


Figure 3. Hadronic shower size spectrum.

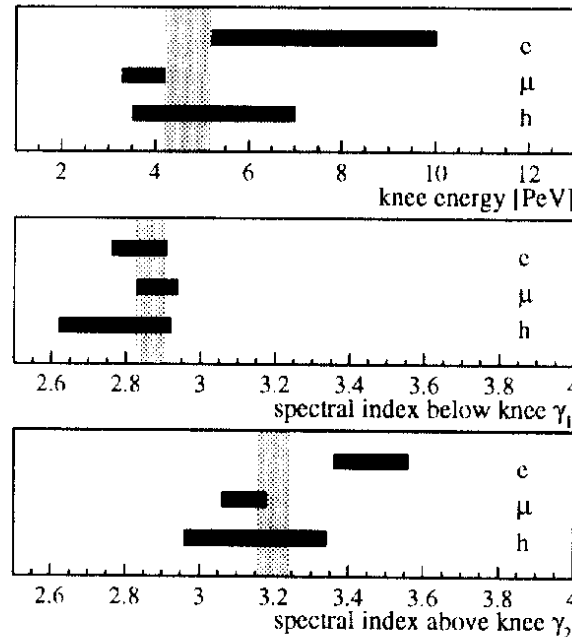
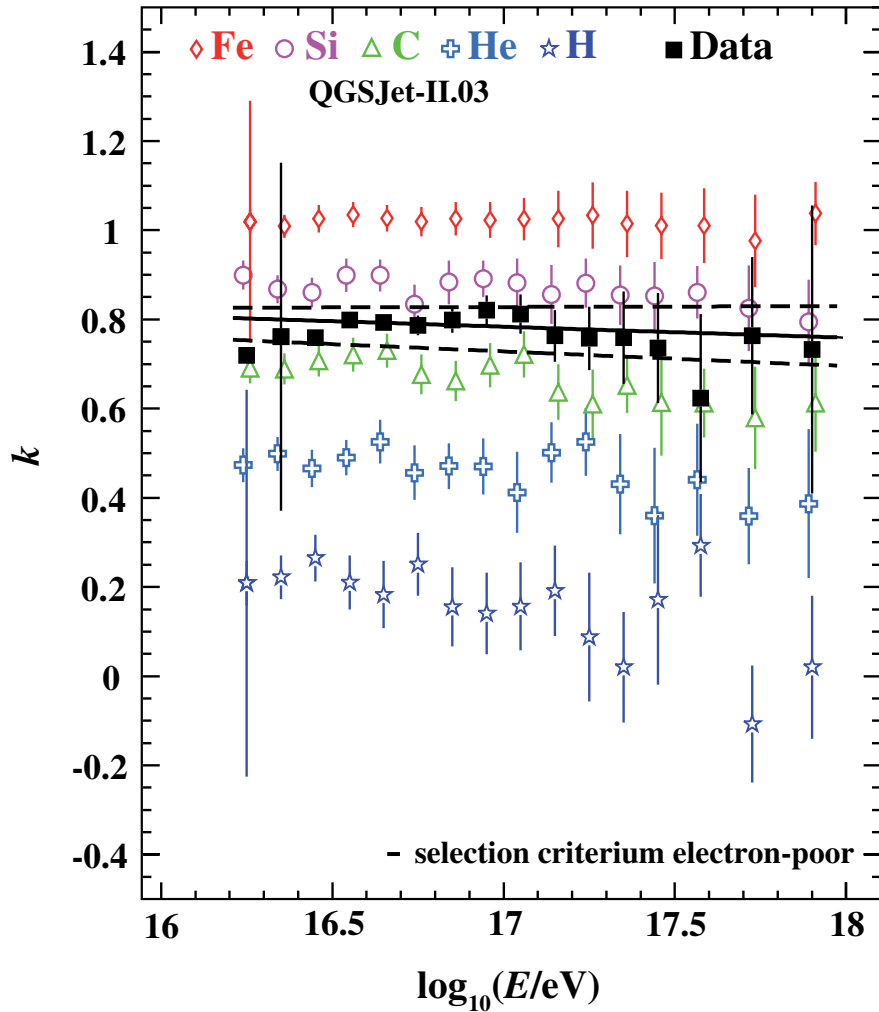


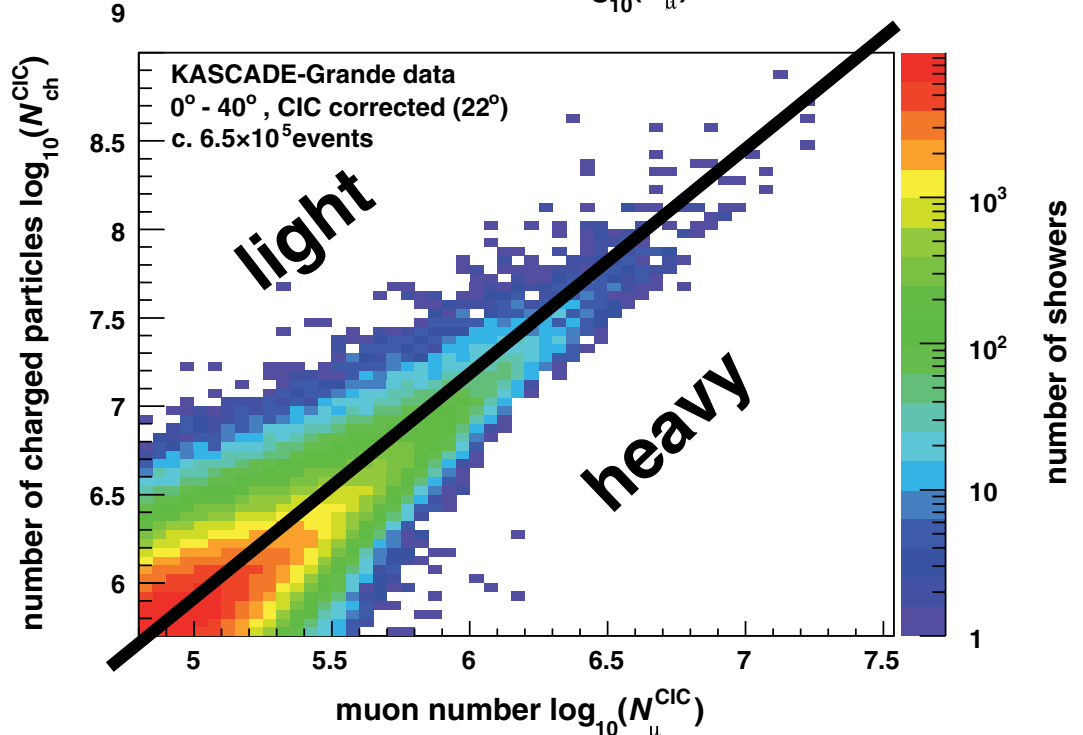
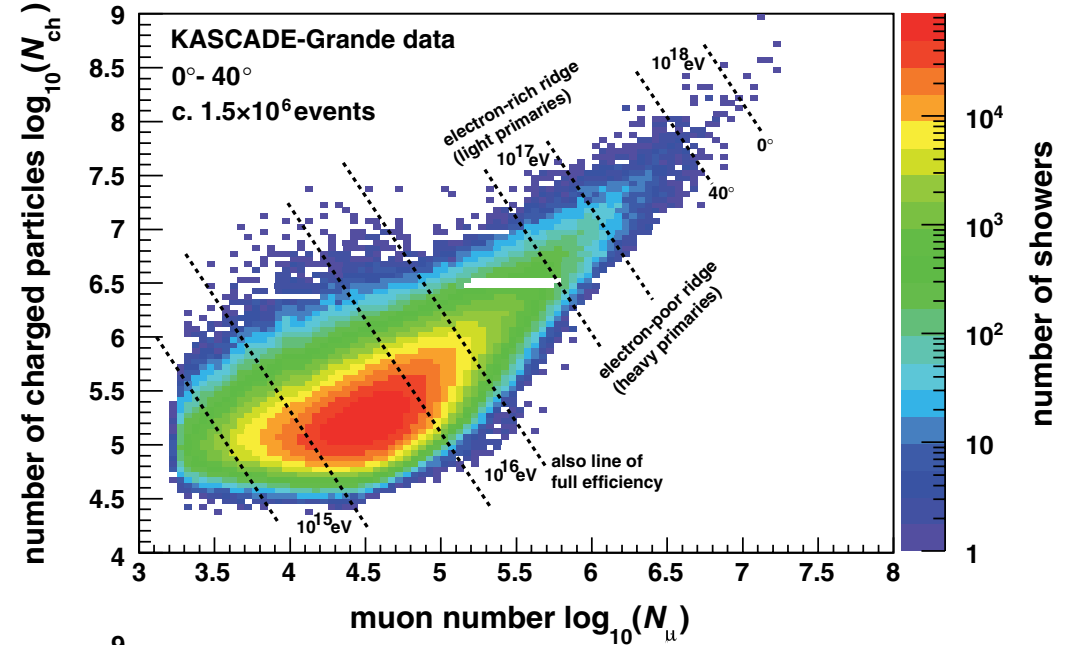
Figure 4. Knee position and spectral indices.

knee observed in all components, electromagnetic, muonic, and hadronic!

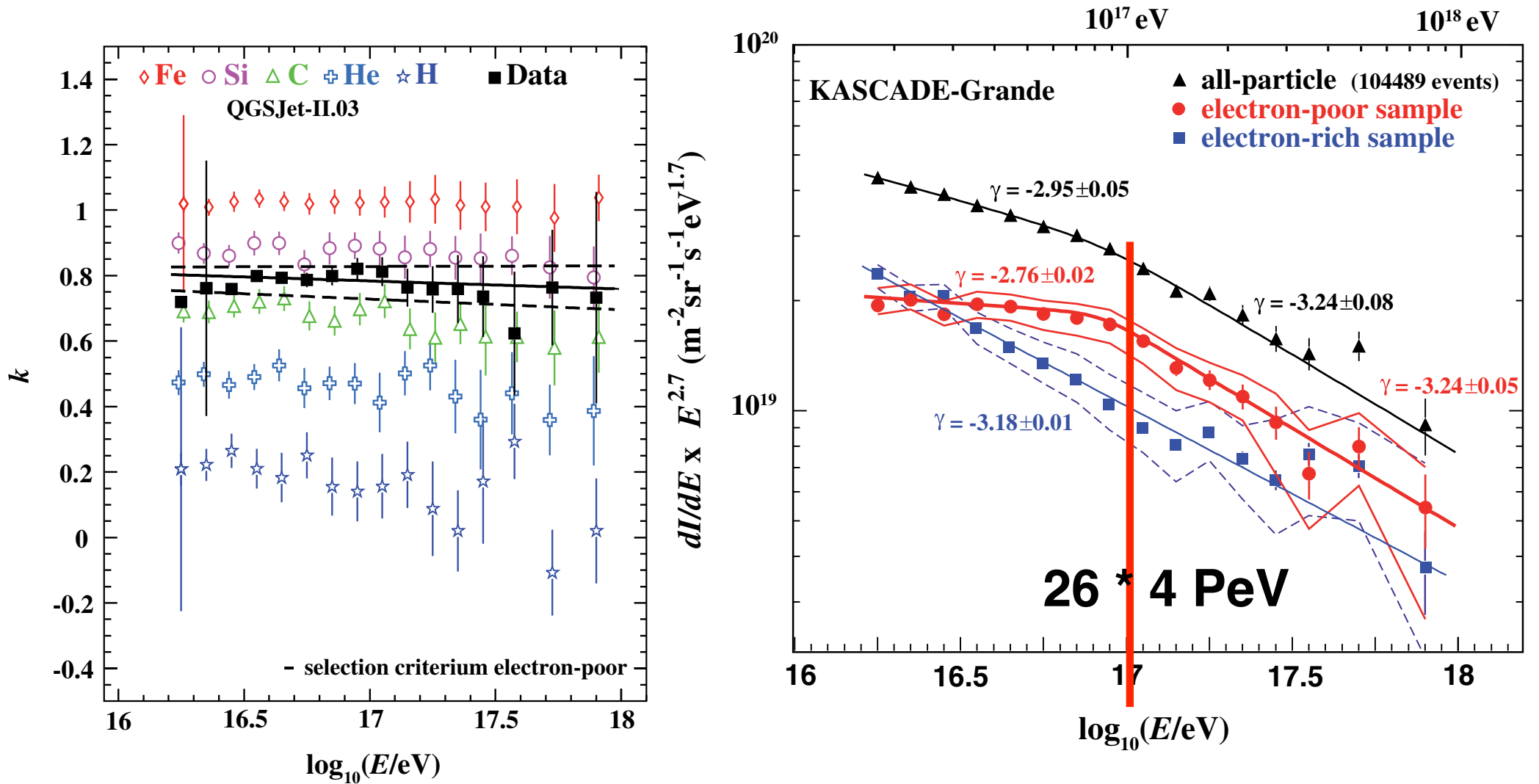
KASCADE-Grande



$$k = \frac{\log_{10}(N_{ch}/N_{\mu}) - \log_{10}(N_{ch}/N_{\mu})_H}{\log_{10}(N_{ch}/N_{\mu})_{Fe} - \log_{10}(N_{ch}/N_{\mu})_H}$$



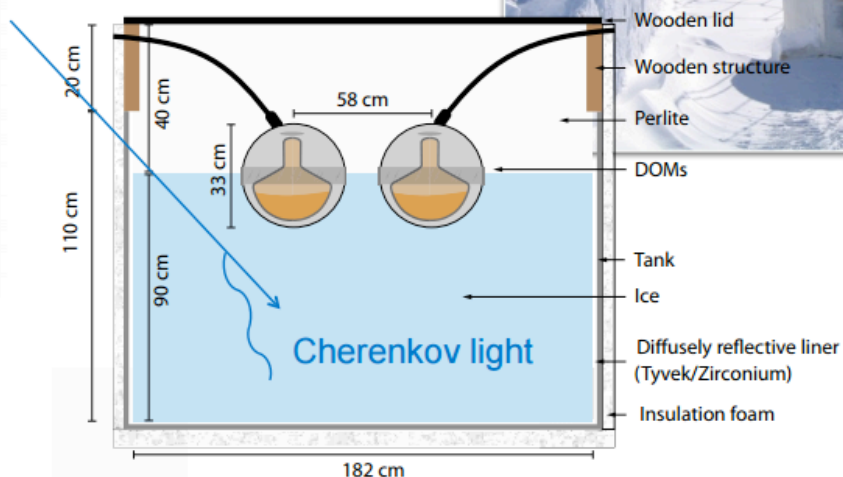
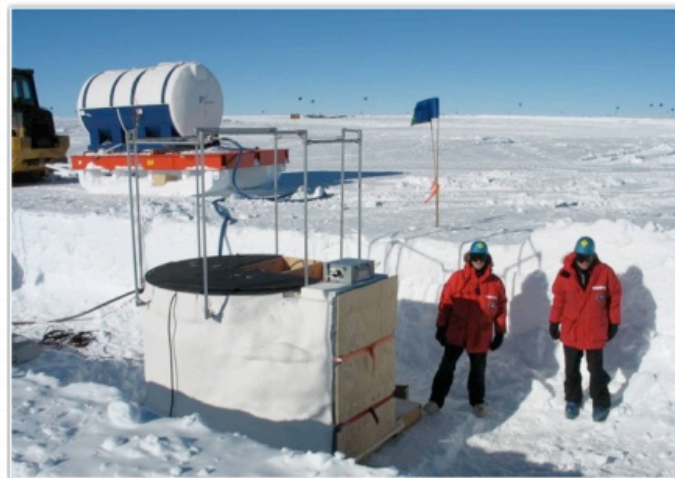
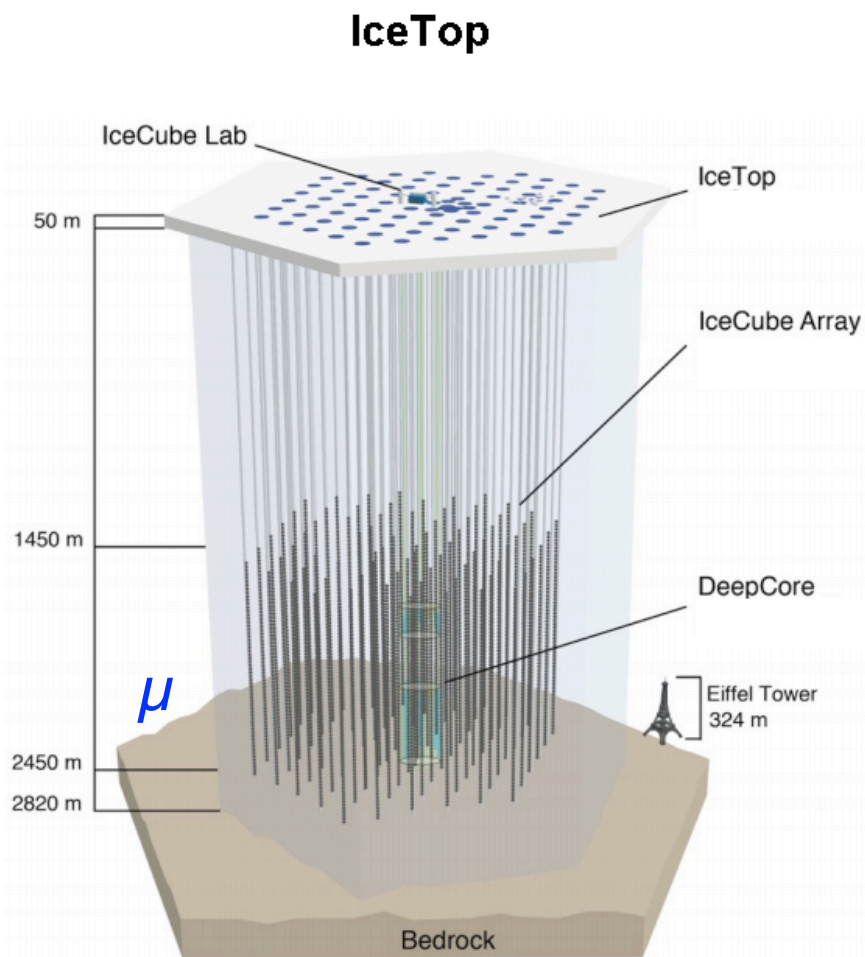
KASCADE-Grande



$$k = \frac{\log_{10}(N_{\text{ch}}/N_{\mu}) - \log_{10}(N_{\text{ch}}/N_{\mu})_{\text{H}}}{\log_{10}(N_{\text{ch}}/N_{\mu})_{\text{Fe}} - \log_{10}(N_{\text{ch}}/N_{\mu})_{\text{H}}}$$

Ice Cube - Ice Top

e/m (+ μ)



*see also
Halzen
ISGR A2024*

Cosmic ray spectrum and composition from PeV to EeV using 3 years of data from IceTop and IceCube

Ice Cube - Ice Top

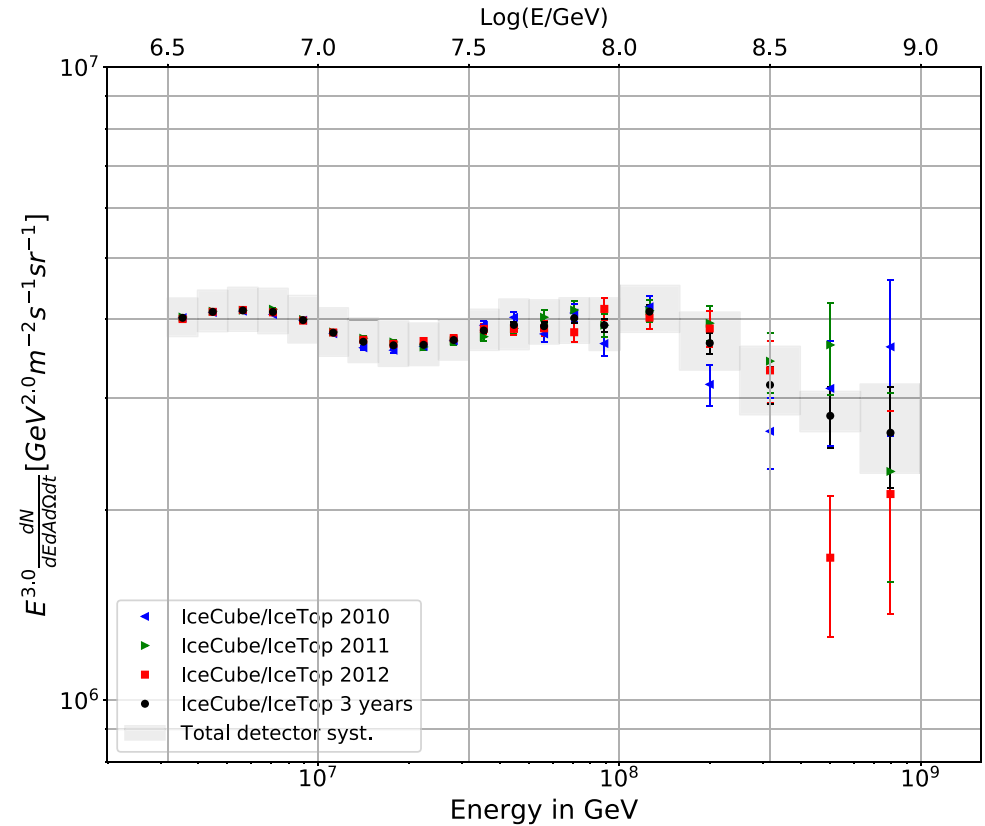
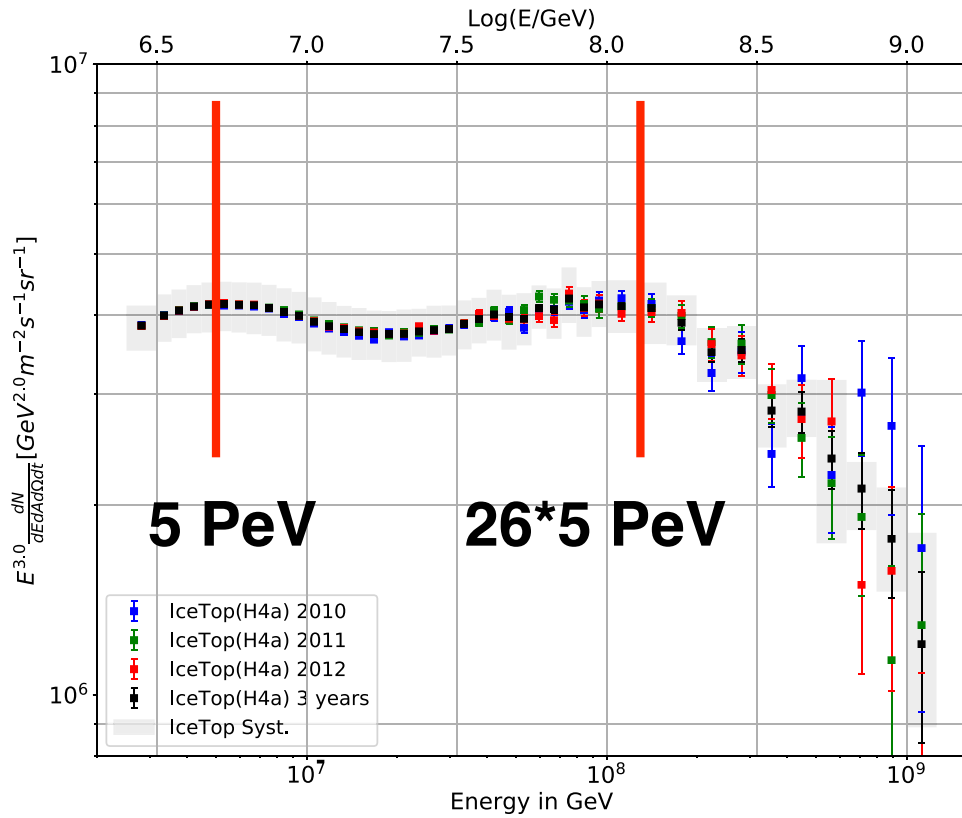


FIG. 9. All-particle energy spectrum from the IceTop-alone analysis from each of the 3 years and the 3 years together.

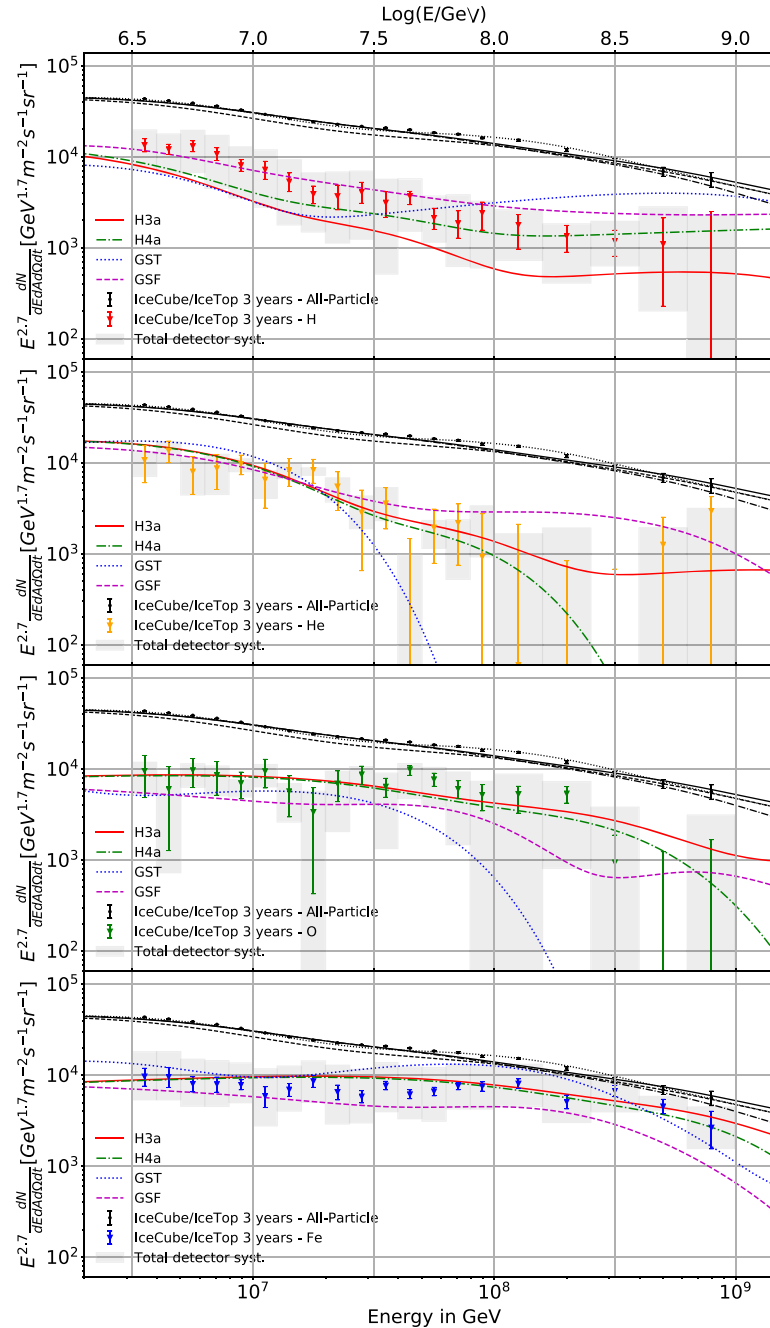
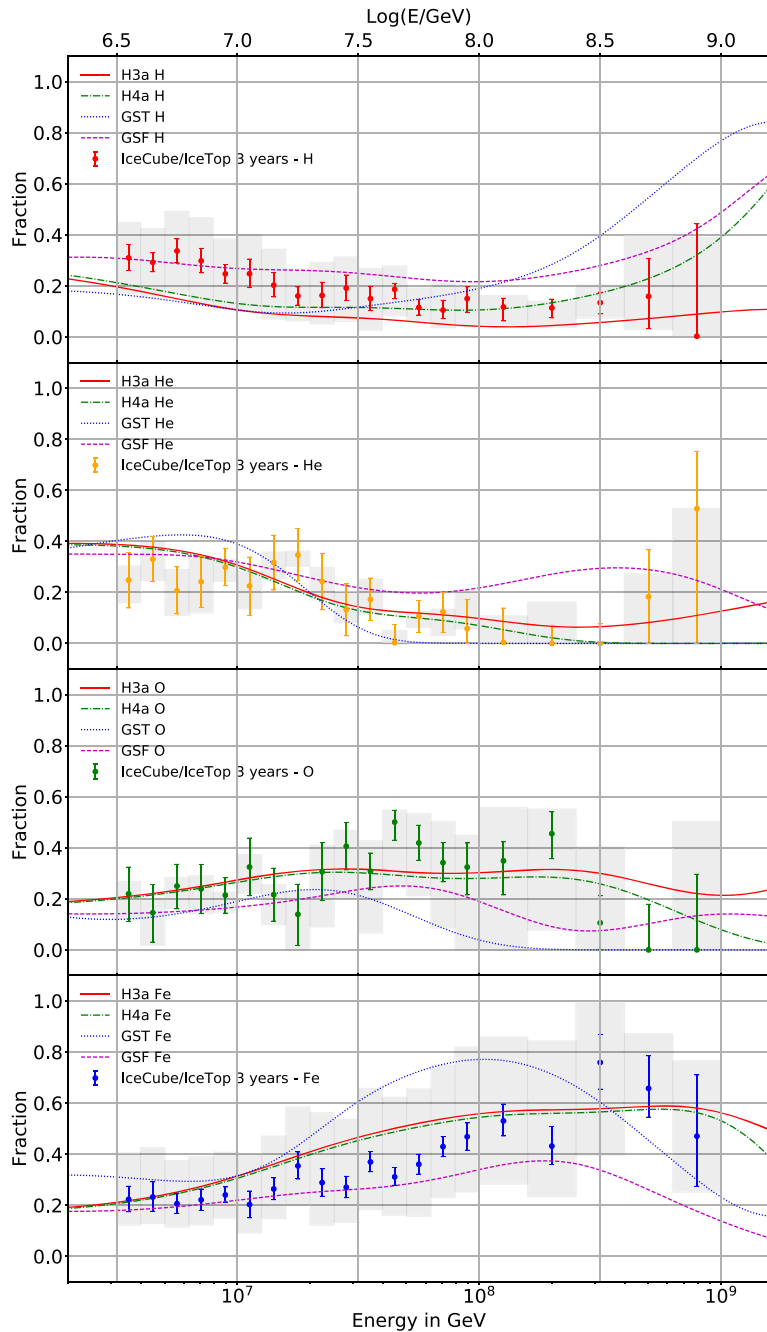
FIG. 12. All-particle energy spectrum from the coincident analysis from each of the 3 years analyzed individually compared to the combined result. The gray band represents the total detector uncertainty from both the IceTop and InIce arrays, as discussed in Sec. IV B.

Ice Top only

combined

Cosmic ray spectrum and composition from PeV to EeV using 3 years of data from IceTop and IceCube

Ice Cube - Ice Top



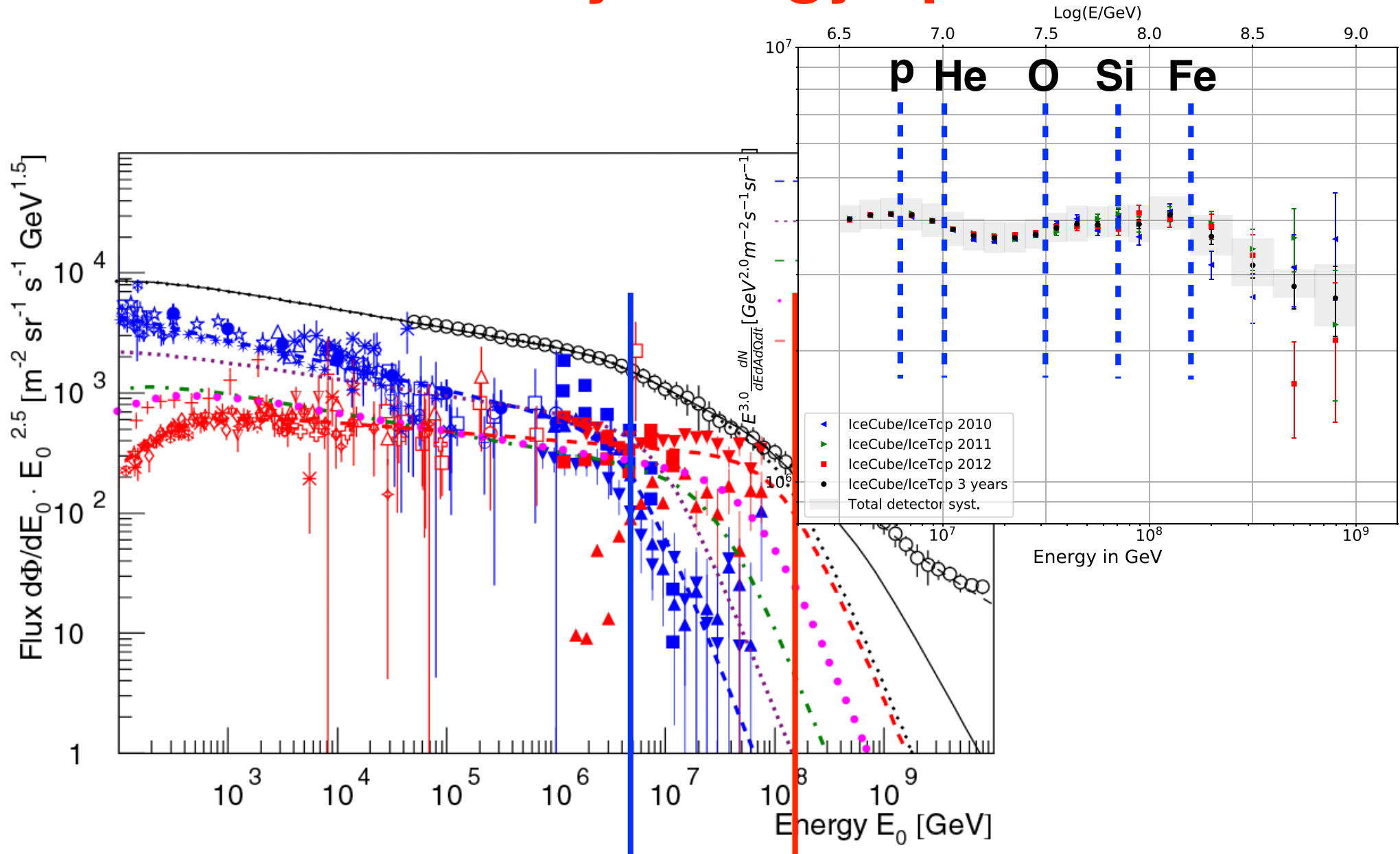
p

He

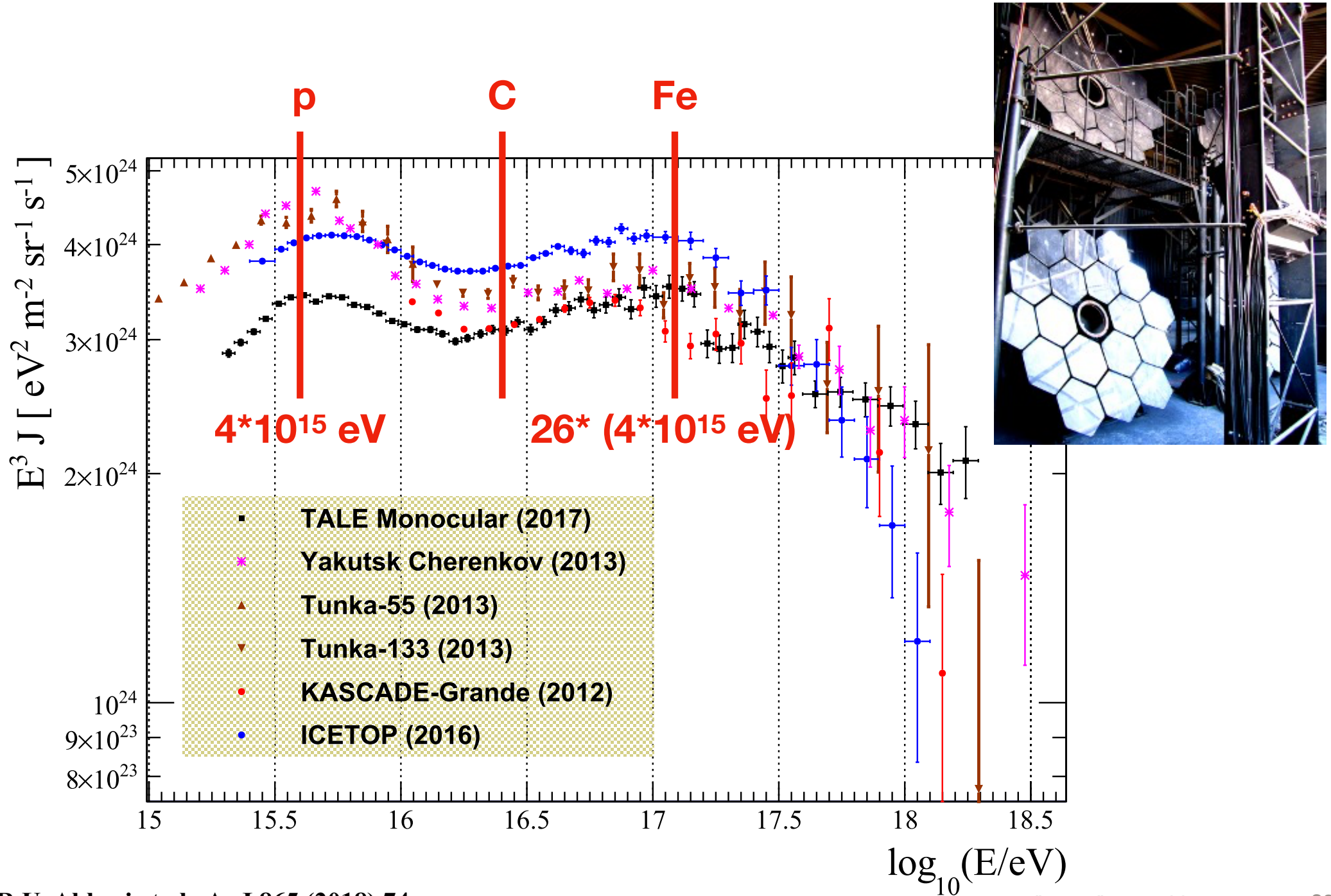
CNO

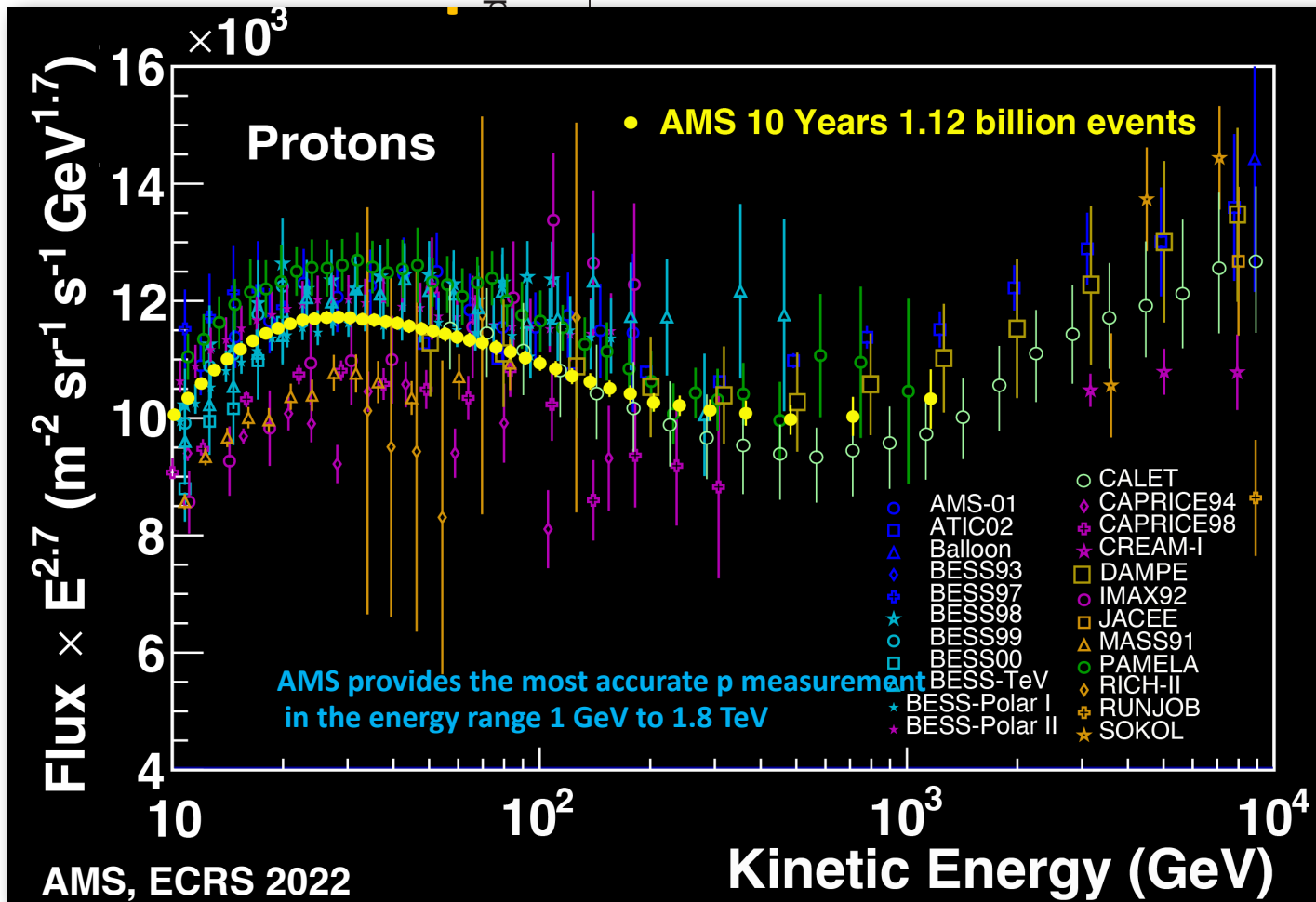
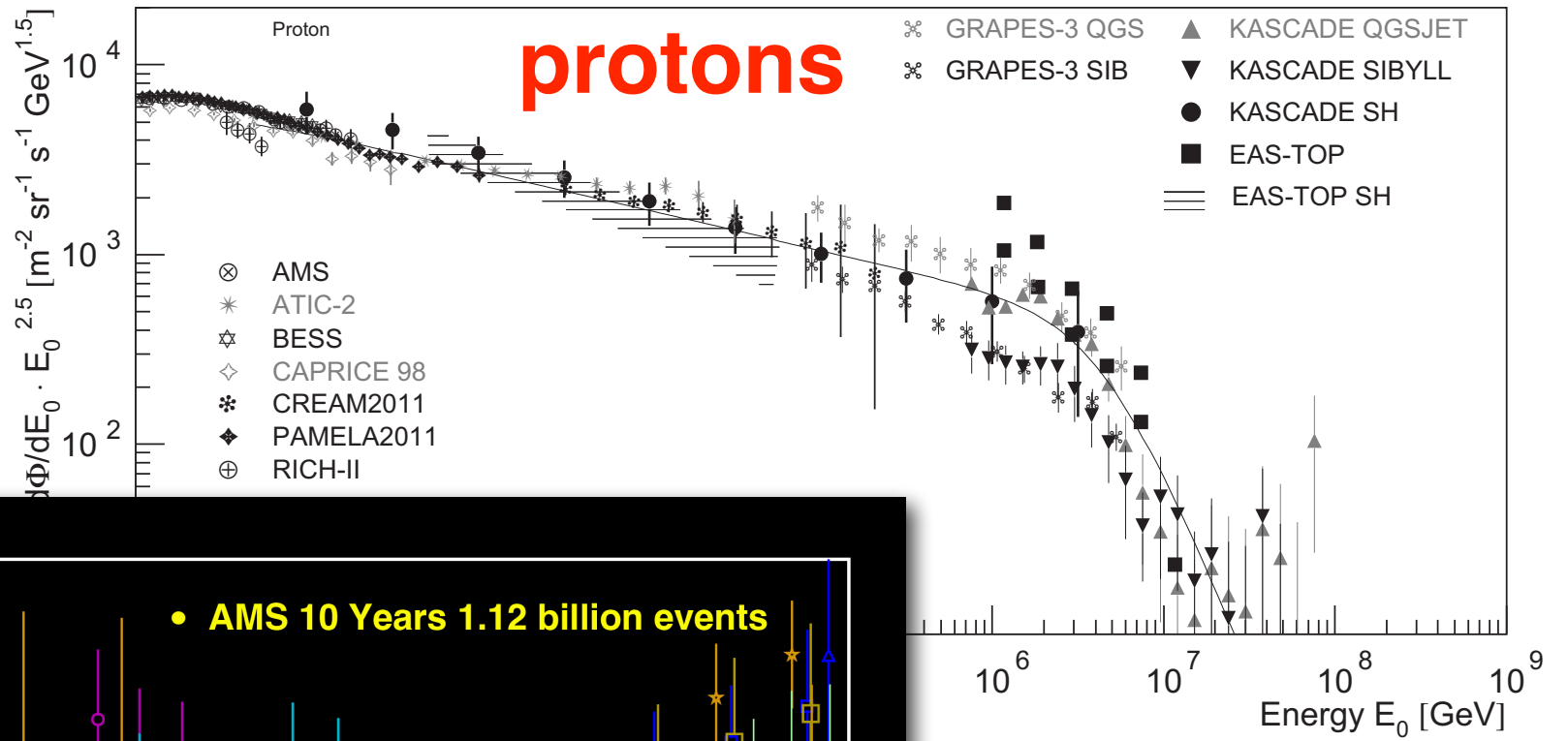
Fe

Cosmic-ray energy spectrum

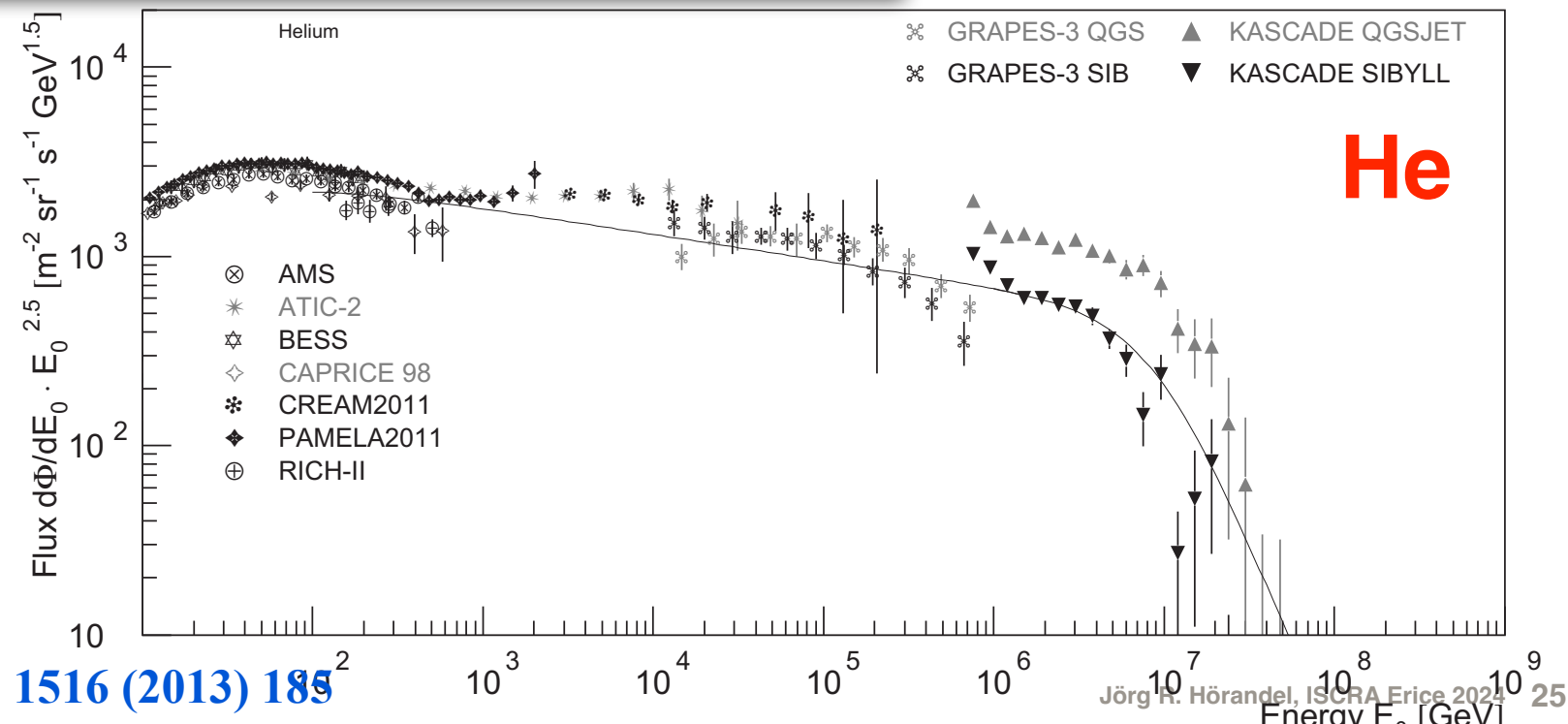
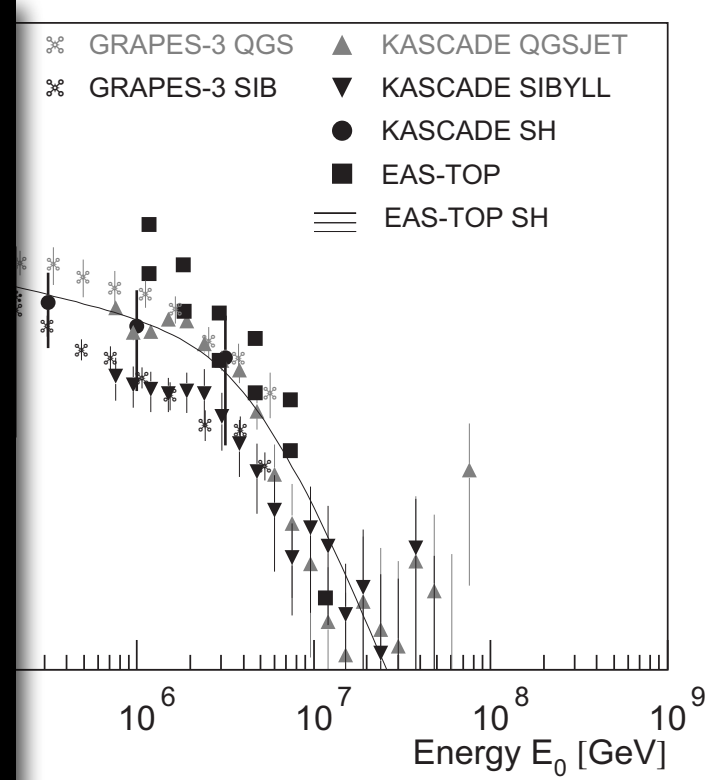
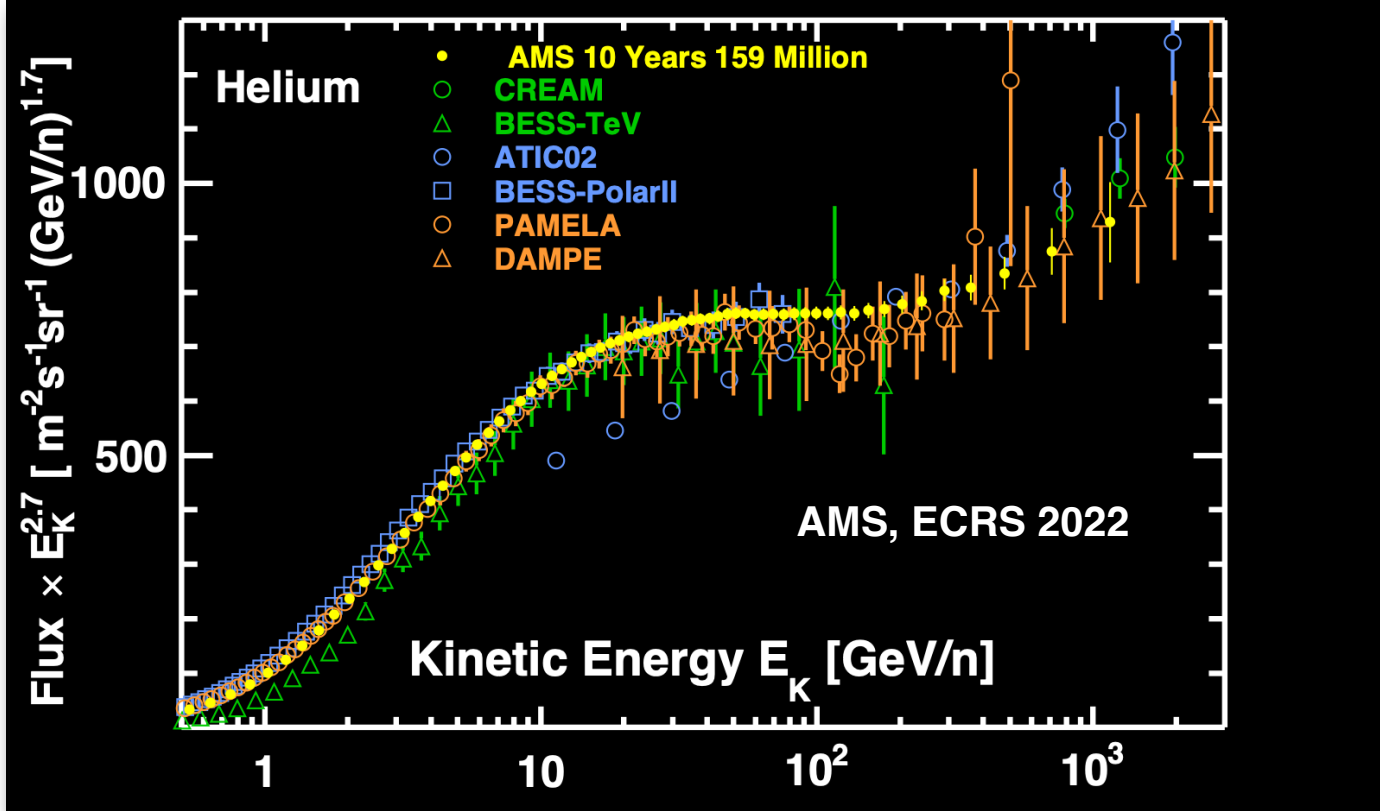


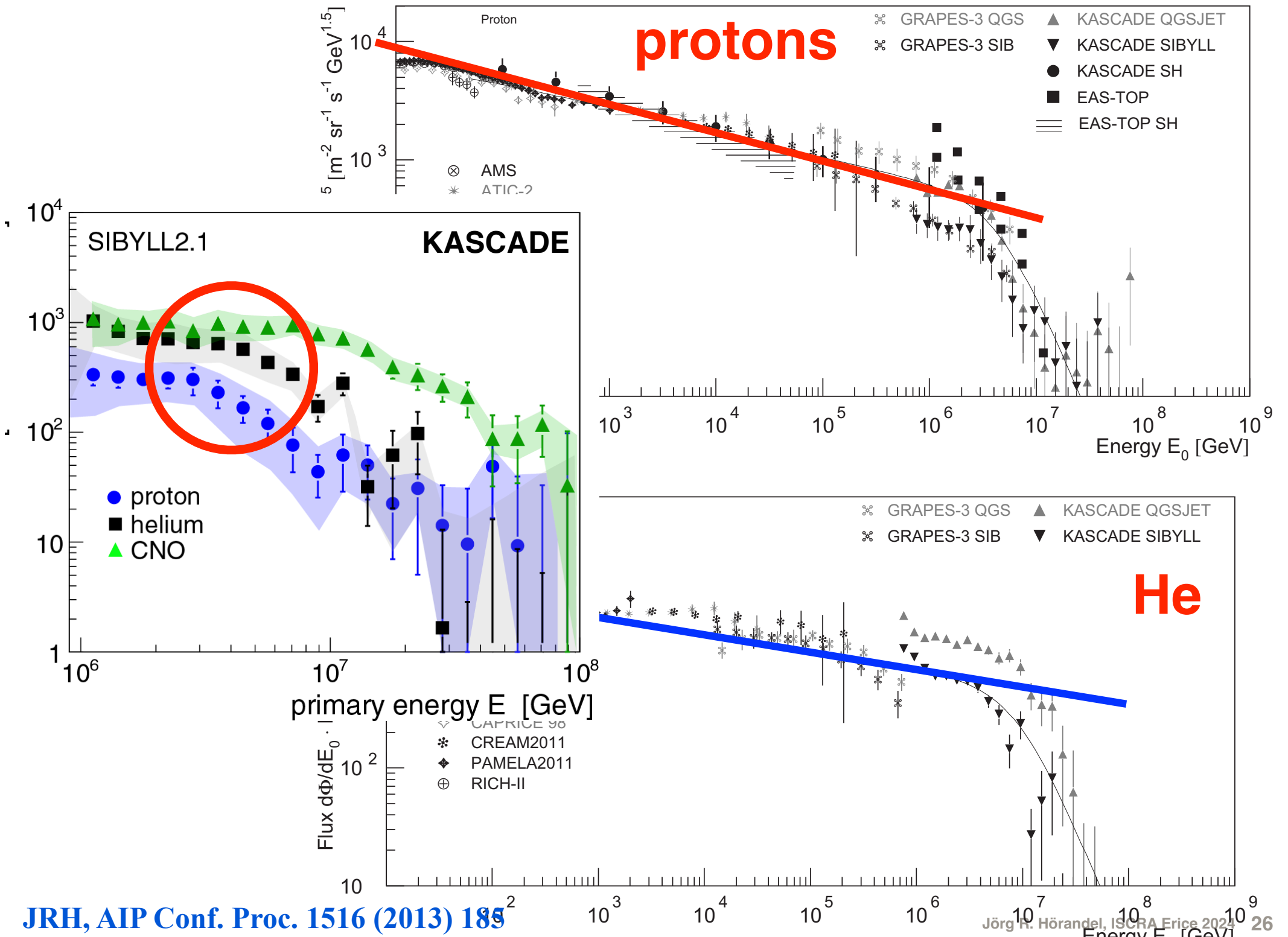
TALE (TA low-energy extension)

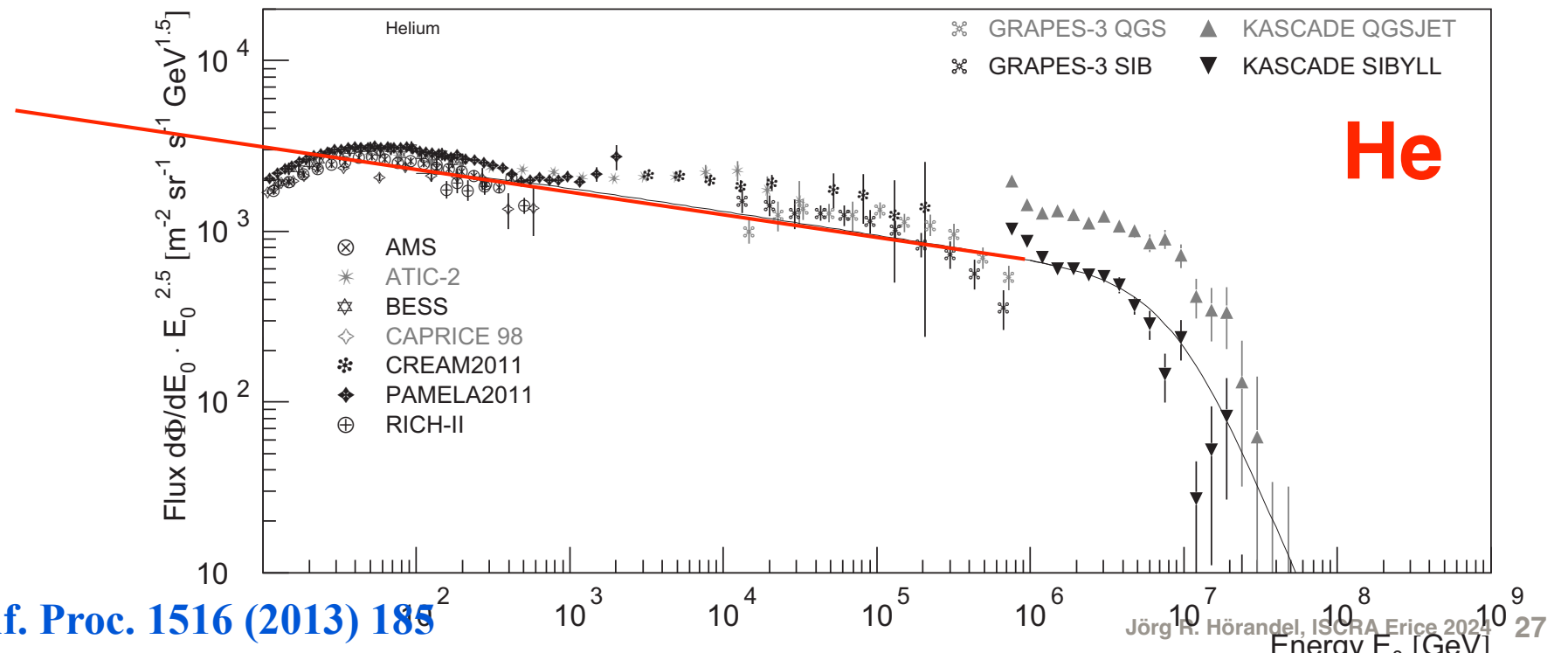
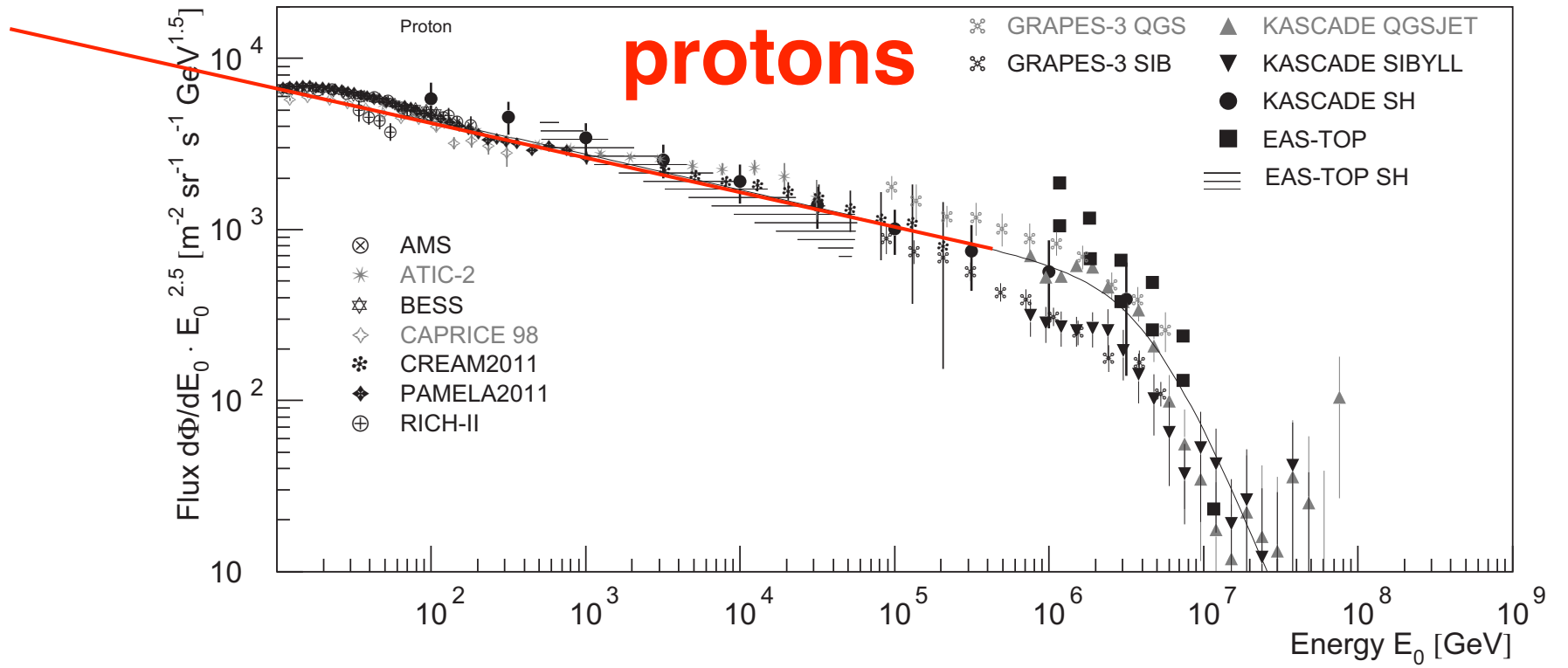


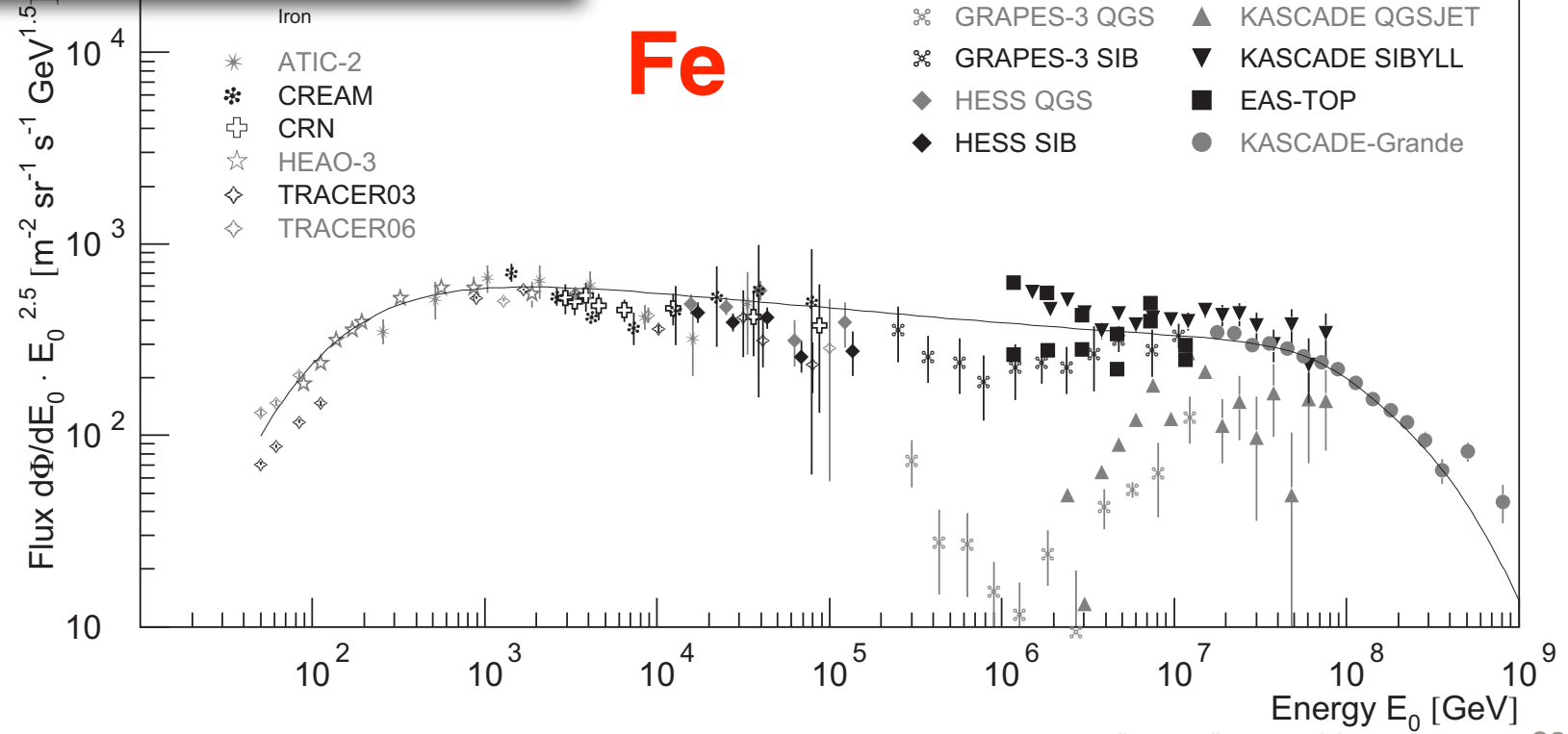
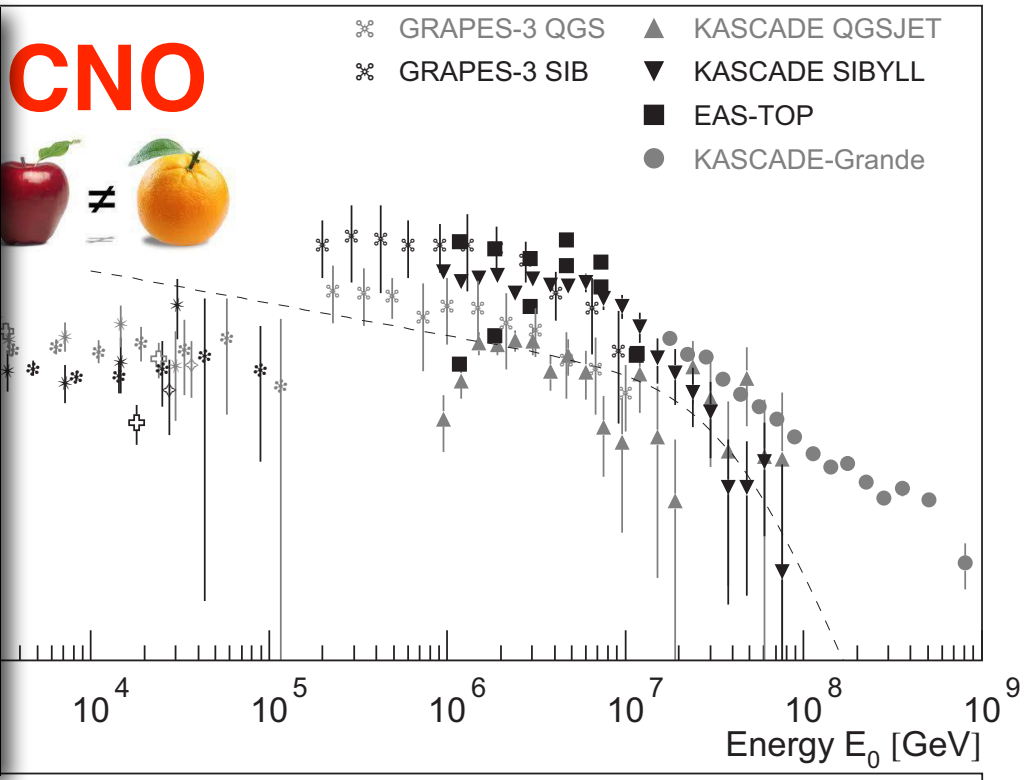
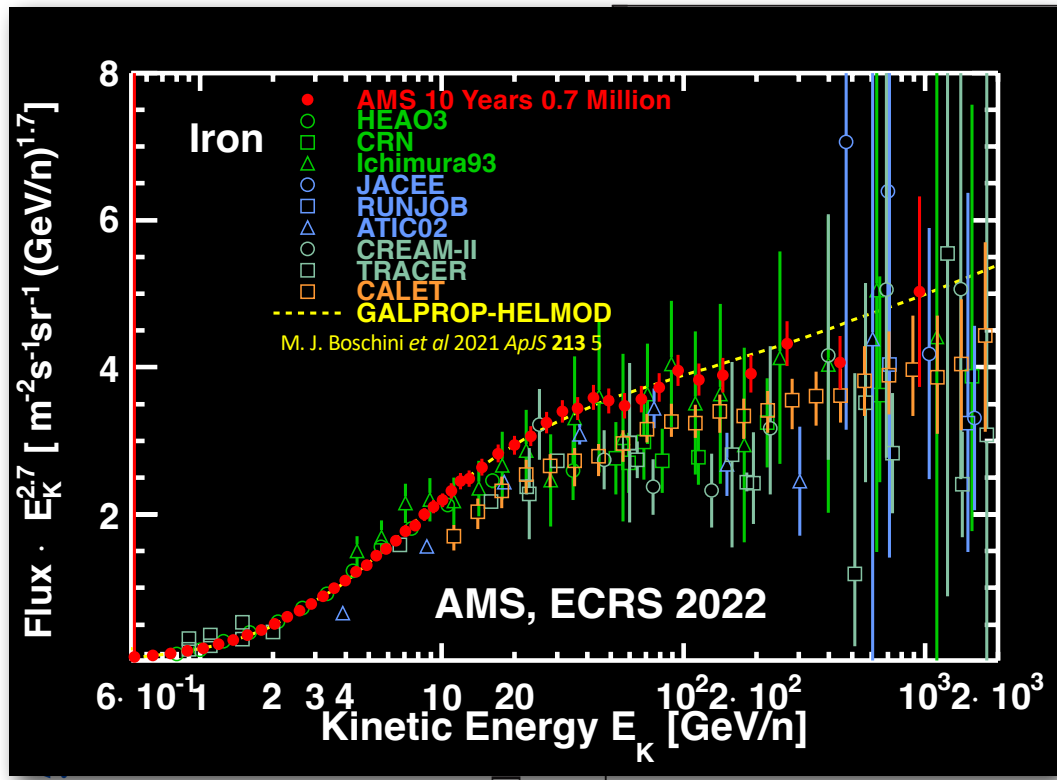


see also
 Sparvoli
 Bernardini
 ISCR A2024









Transport equation for cosmic rays in the Galaxy

*see also
Evoli
ISCR A2024*

diffusion

energy loss (Bethe Bloch)

loss through interactions
with ISM (spallation)

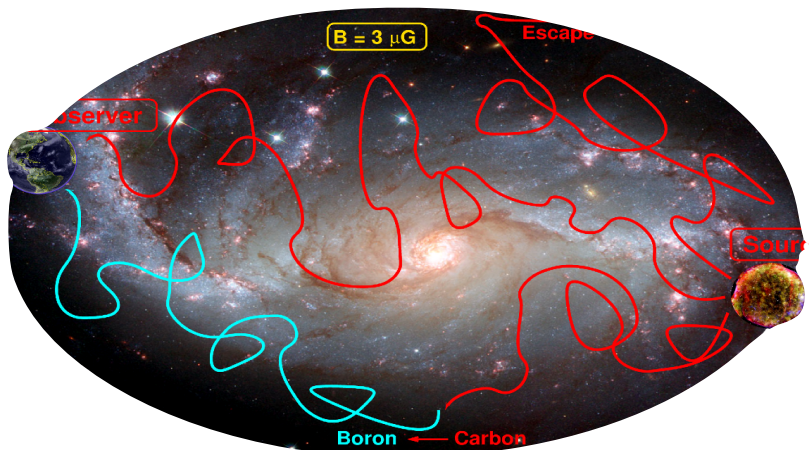
loss through radioactive decay

$$\frac{\partial N_i}{\partial t} = \nabla(D_i \nabla N_i) - \frac{\partial}{\partial E}(b_i N_i) - n\nu\sigma_i N_i - \frac{N_i}{\gamma\tau_i} + Q_i + \sum_{j>i} n\nu\sigma_{ij} N_j + \sum_{j>i} \frac{N_j}{\gamma_j\tau_{ij}}$$

source term

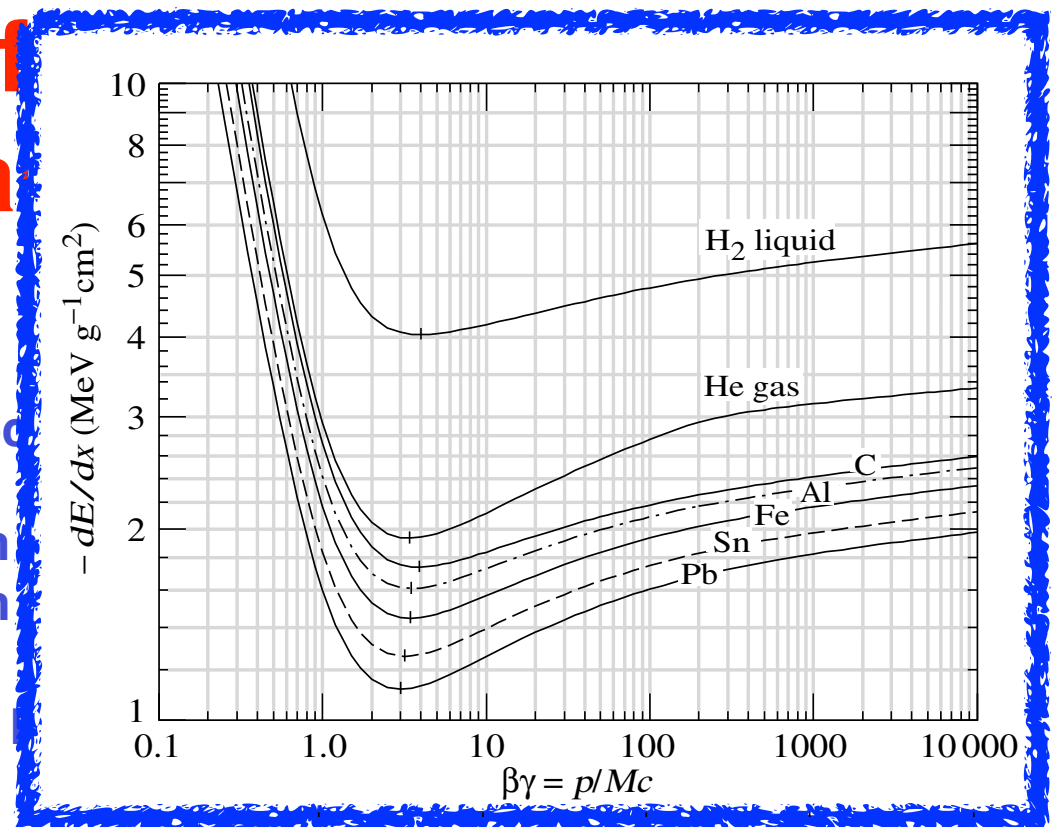
production through spallation
of heavy nuclei

production through decay
of heavy nuclei



Transport equation for Galactic Cosmic Rays

Galactic



diffusion

energy loss (Bethe Bloch)

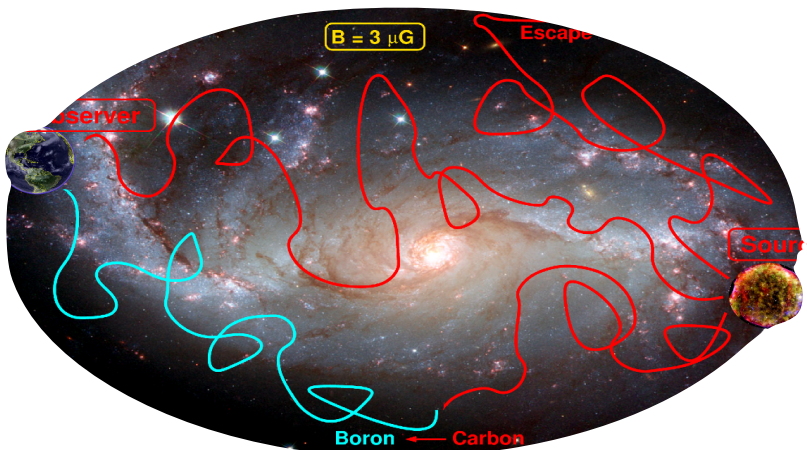
loss through with

$$\frac{\partial N_i}{\partial t} = \nabla(D_i \nabla N_i) - \frac{\partial}{\partial E} (E N_i) - n\nu\sigma_i N_i - \frac{N_i}{\gamma\tau_i} + Q_i + \sum_{j>i} n\nu\sigma_{ij} N_j + \sum_{j>i} \frac{N_j}{\gamma_j\tau_{ij}}$$

source term

production through spallation of heavy nuclei

production through decay of heavy nuclei



Transport equation for cosmic rays in the Galaxy

diffusion

energy loss (Bethe Bloch)

loss through interactions with ISM (spallation)

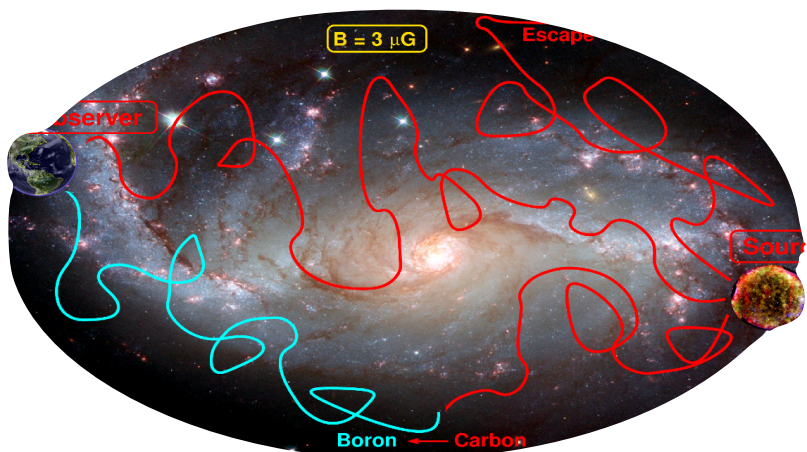
loss through radioactive decay

$$\frac{\partial N_i}{\partial t} = \nabla(D_i \nabla N_i) - \frac{\partial}{\partial E} (D_i N_i) - n\nu\sigma_i N_i - \frac{N_i}{\gamma\tau_i} + Q_i + \sum_{j>i} n\nu\sigma_{ij} N_j + \sum_{j>i} \frac{N_j}{\gamma_j\tau_{ij}}$$

source term

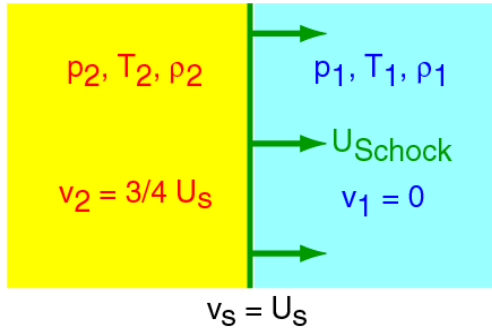
production through spallation of heavy nuclei

production through decay of heavy nuclei

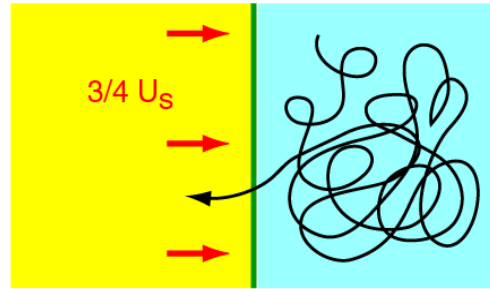


1st order Fermi acceleration at strong shock

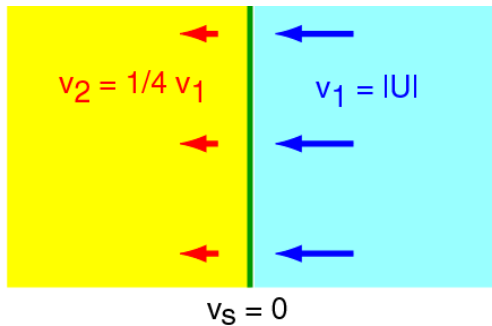
a) rest system of unshocked ISM | ISM



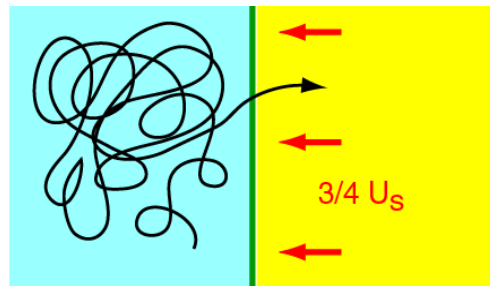
b) rest system of unshocked ISM



c) rest system of shock front

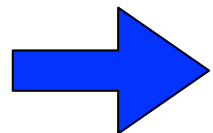


d) rest system of shocked ISM



energy gain

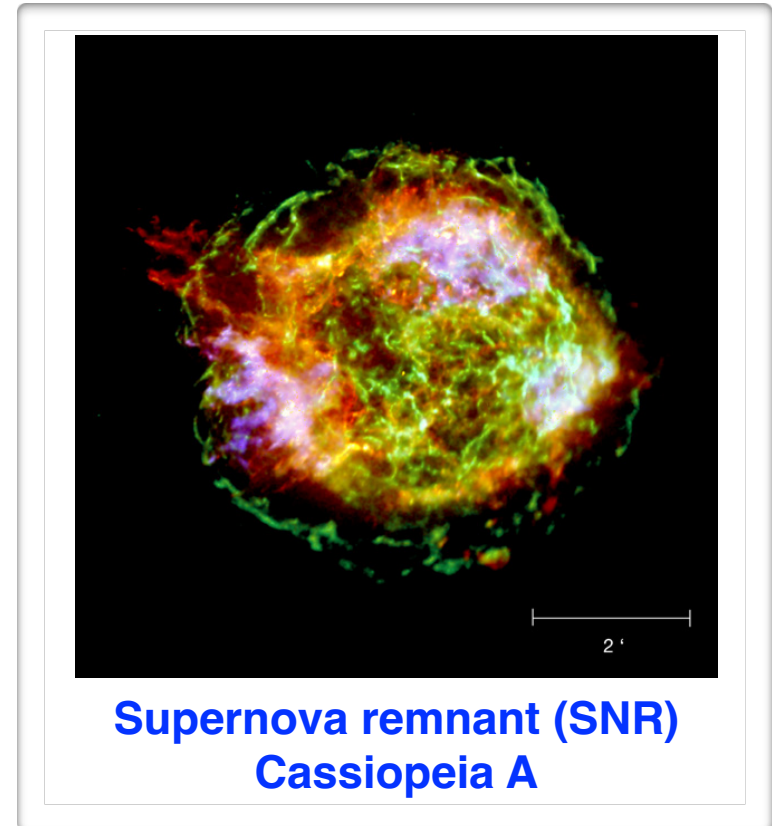
$$\frac{\Delta E}{E} \propto \frac{U_s}{c}$$



$$N(E) dE \propto E^{-2} dE$$

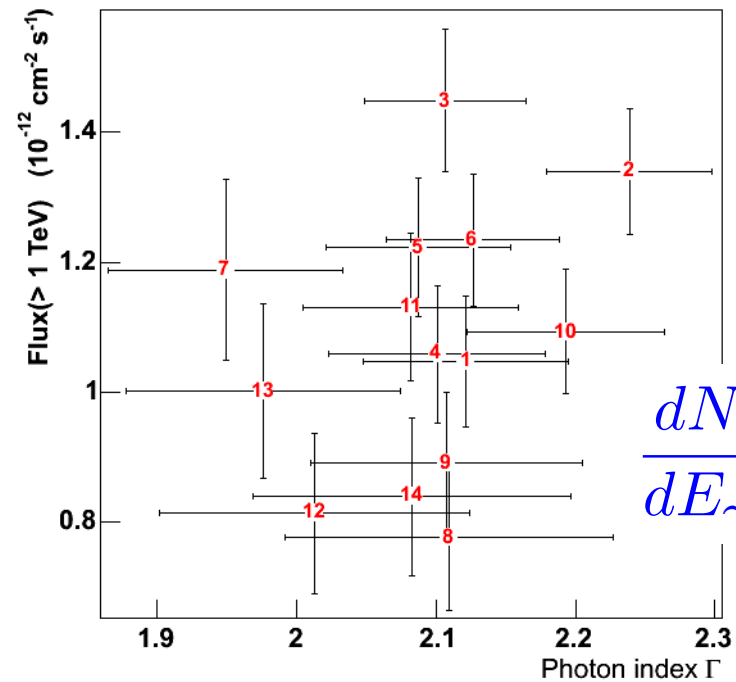
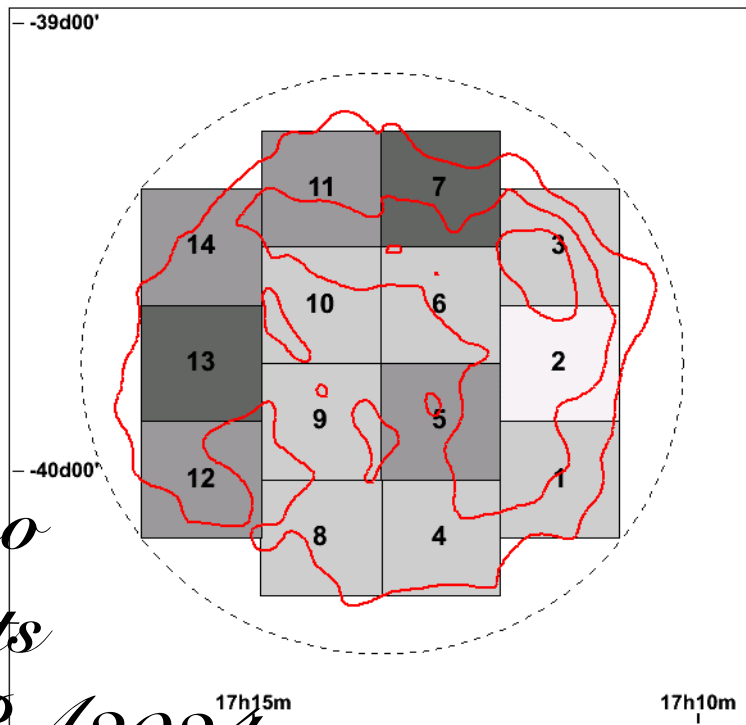
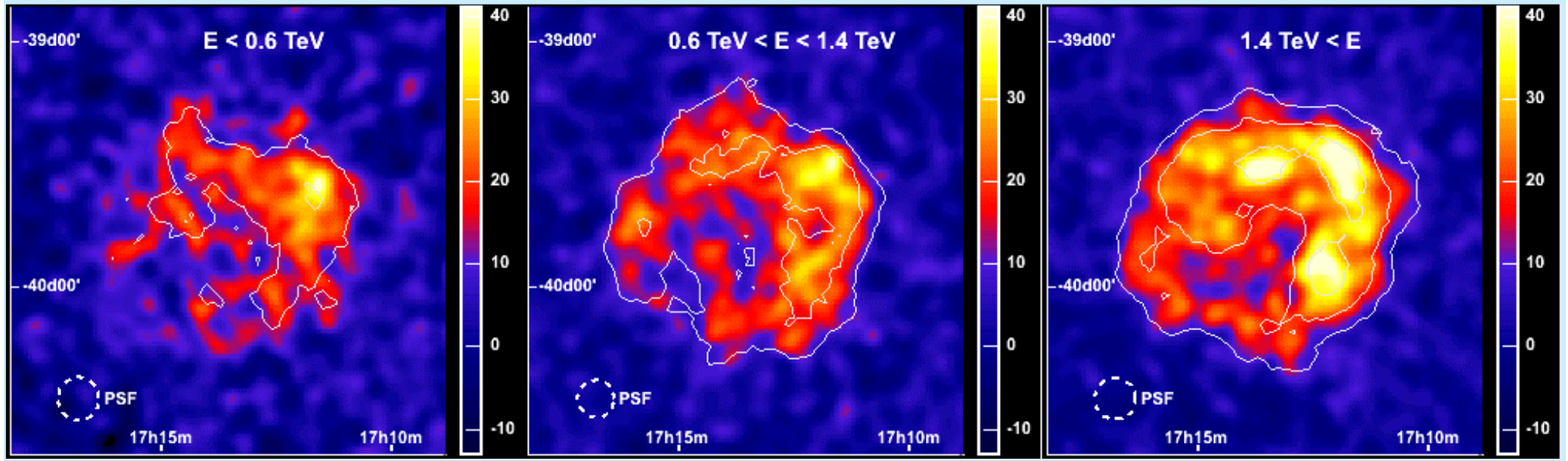
power law with spectral index
-2.0 ... -2.1

Bell, Blanford, Ostriker (1978)



Supernova remnant (SNR)
Cassiopeia A

H.E.S.S. supernova remnant RXJ 1713



$$\frac{dN}{dE_\gamma} \propto E_\gamma^{-\Gamma}$$

*see also
Egberts
ISCR 2024*

Ultrahigh-energy photons up to 1.4 petaelectronvolts from 12 γ -ray Galactic sources

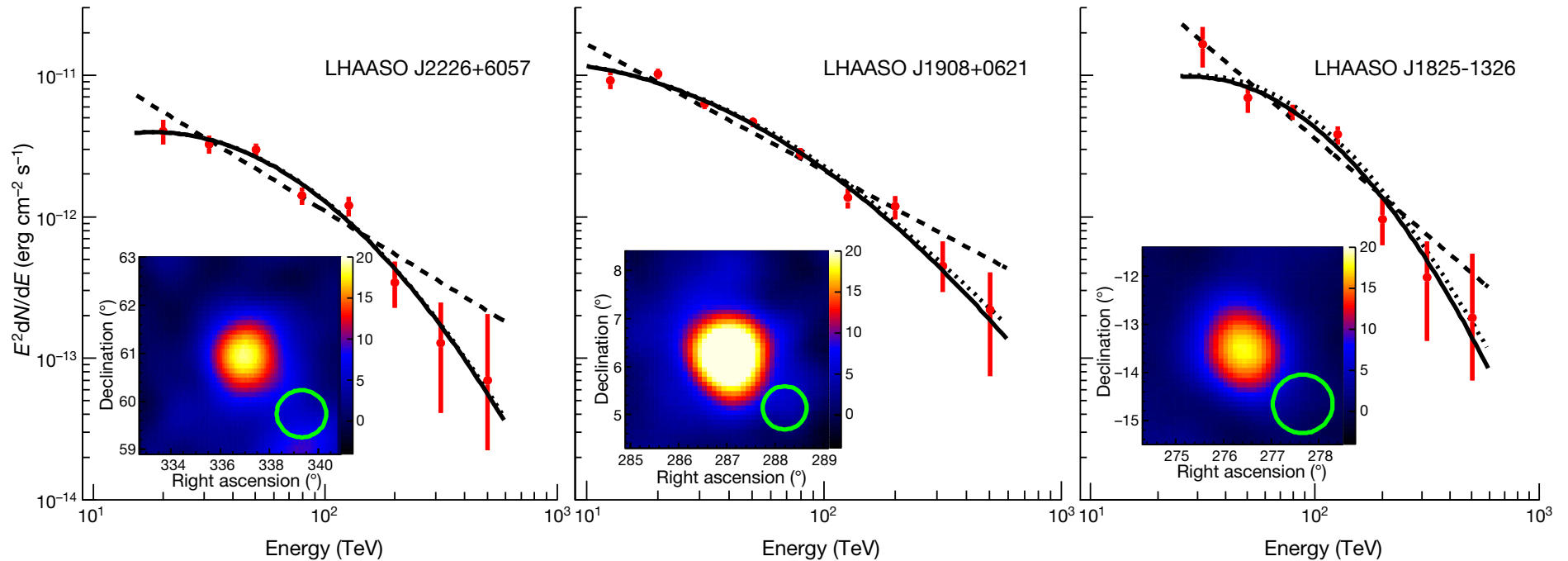


Fig. 1 | Spectral energy distributions and significance maps. a–c, Data are shown for LHAASO J2226+6057 (a), LHAASO J1908+0621 (b), and LHAASO J1825-1326 (c). Spectral fits with a log-parabola function (solid lines) in the form of $[E/(10 \text{ TeV})]^{-a-b \log[E/(10 \text{ TeV})]}$ are compared with the power-law fits $E^{-\Gamma}$ for: $a=1.56$, $b=0.88$ and $\Gamma=3.01$ (a); $a=2.27$, $b=0.46$ and $\Gamma=2.89$ (b); and $a=0.92$, $b=1.19$ and $\Gamma=3.36$ (c). The dotted curves correspond to the log-parabola fits corrected for the interstellar γ - γ absorption (see Methods for the radiation fields and Extended Data Fig. 6 for the opacity curves). The comparison of the power-law (PL) model and the log-parabola (LOG) model with the Akaike Information Criterion²⁰ (AIC) gives: $\text{AIC}_{\text{LOG}}=12.3$ and $\text{AIC}_{\text{PL}}=24.4$ for LHAASO J2226+6057; $\text{AIC}_{\text{LOG}}=15.1$ and $\text{AIC}_{\text{PL}}=30.1$ for LHAASO J1908+0621; and

$\text{AIC}_{\text{LOG}}=11.6$ and $\text{AIC}_{\text{PL}}=14.8$ for LHAASO J1825-1326. The insets show the significance maps of the three sources, obtained for γ -rays above 25 TeV. The colour bars show the square root of test statistics (TS), which is equivalent to the significance. The significance ($\sqrt{\text{TS}}$) maps are smoothed with the Gaussian-type point spread function (PSF) of each source. The size of PSFs (68% contamination regions) are shown at the bottom right of each map. We note that the PSFs of the three sources are slightly different owing to different inclination angles. Namely, the 68% contamination angles are 0.49° for LHAASO J2226+6057, 0.45° for LHAASO J1908+0621 and 0.62° for LHAASO J1825-1326. Error bars represent one standard deviation.

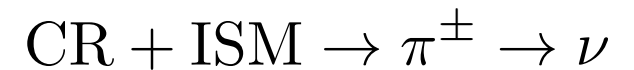
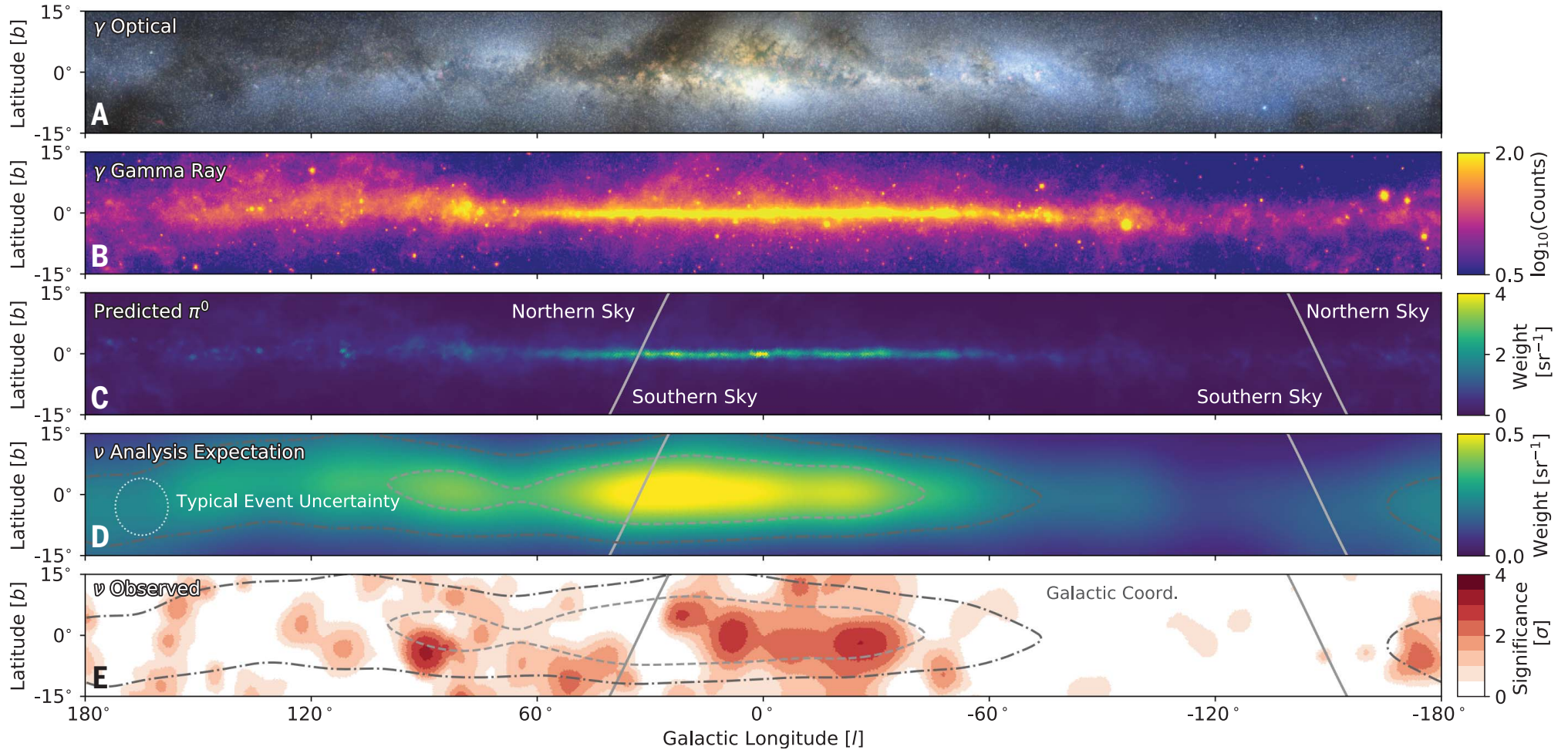
$$\text{CR} + \text{ISM} \rightarrow \pi^0 \rightarrow \gamma$$

also ambiguities due to e/m channels

Observation of high-energy neutrinos from the Galactic plane

IceCube Collaboration*†

*see also
Halzen
ISCR A2024*



general considerations about accelerators

trajectory of particle in B field

centripetal force = Lorentz force

$$m \frac{v^2}{r} = q \cdot v \cdot B \quad m \cdot v = p \quad \text{momentum}$$

$$\frac{p}{r} = Z \cdot e \cdot B$$

$$r_L = \frac{p}{z \cdot e \cdot B} \quad \text{Larmor radius}$$

L dimension of accelerator

$$L > 2 r_L$$

closer look (Hillas 1984): $L > \frac{2r_L}{\beta}$

velocity of scattering centers $\beta = \frac{v}{c}$

$$L > \frac{2 \cdot p}{z \cdot e \cdot B \cdot \beta}$$



$$B \cdot L > \frac{2 \cdot p}{z \cdot e \cdot \beta}$$

Hillas criterion

in astrophysical units

$$r_L = 1.08 \text{ pc} \frac{E_{15}}{Z \cdot B_{\mu G}}$$

$$B_{\mu G} \cdot L_{pc} > \frac{2 \cdot E_{15}}{Z \cdot \beta}$$

**necessary condition
not sufficient**

$$E_{15} < Z \cdot B_{\mu G} \cdot L_{pc} \cdot \frac{\beta}{2}$$

Contribution of (regular) SNR-CR

$$E_c = Z \cdot 4.5 \cdot 10^6 \text{ GeV}$$

$$Q(p) = A Q_0 (A p)^{-q} \exp\left(-\frac{A p}{Z p_c}\right),$$

Table 1. Source spectral indices, q , and energy injected per supernova, f , for the different species of cosmic rays used in the calculation of the SNR-CRs spectra shown in Figures 1 and 2.

Particle type	q	f ($\times 10^{49}$ ergs)
Proton	2.24	6.95
Helium	2.21	0.79
Carbon	2.21	2.42×10^{-2}
Oxygen	2.25	2.52×10^{-2}
Neon	2.25	3.78×10^{-3}
Magnesium	2.29	5.17×10^{-3}
Silicon	2.25	5.01×10^{-3}
Iron	2.25	4.95×10^{-3}

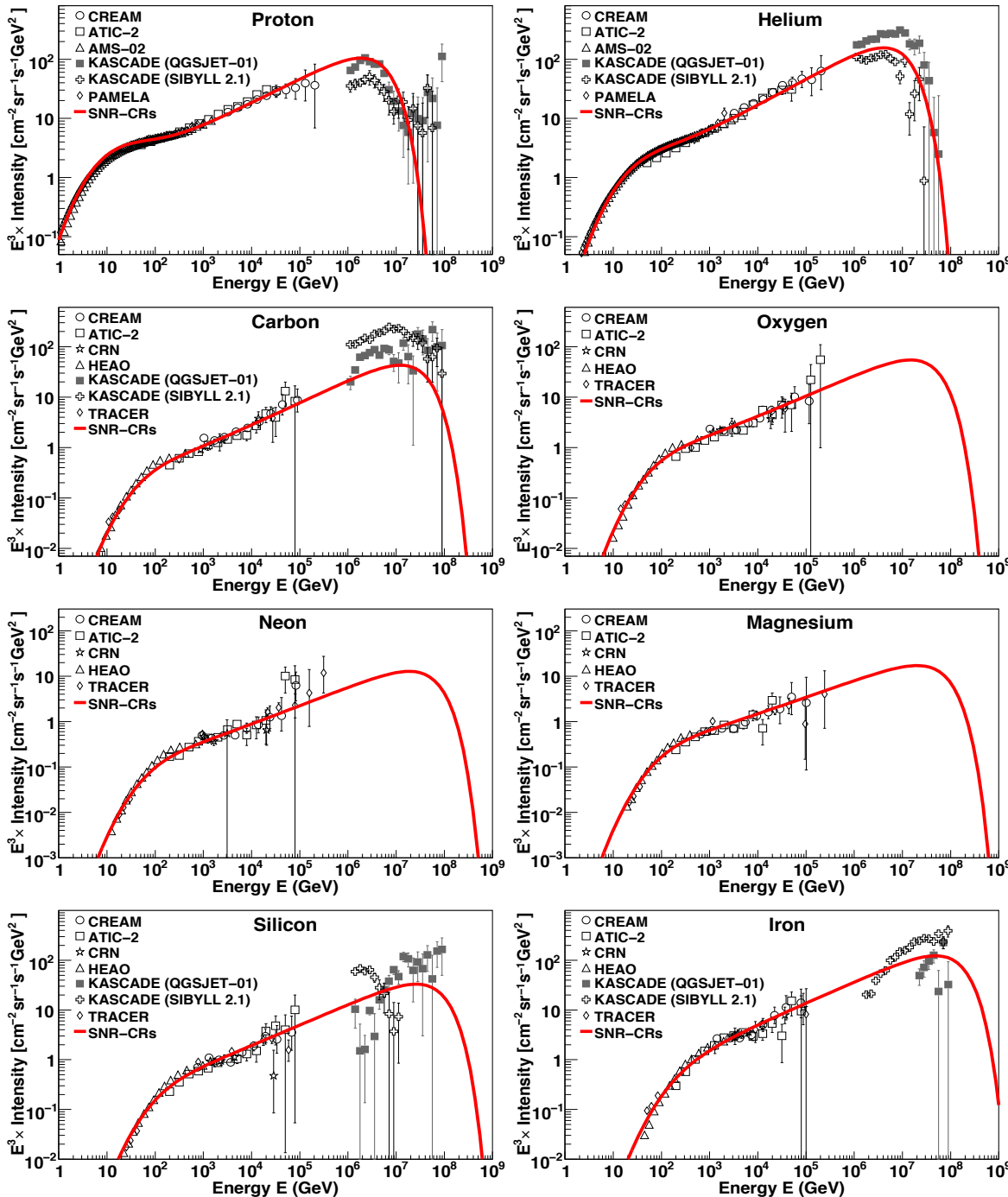
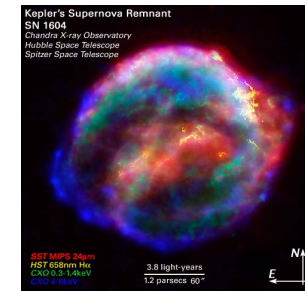


Fig. 1. Energy spectra for different cosmic-ray elements. *Solid line*: Model prediction for the SNR-CRs. *Data*: CREAM (Ahn et al. 2009; Yoon et al. 2011), ATIC-2 (Panov et al. 2007), AMS-02 (Aguilar et al. 2015a,b), PAMELA (Adriani et al. 2011), CRN (Müller et al. 1991; Swordy et al. 1990), HEAO (Engelmann et al. 1990), TRACER (Obermeier et al. 2011), and KASCADE (Antoni et al. 2005). Cosmic-ray source parameters (q, f) used in the calculation are given in Table 1. For the other model parameters (D_0, a, η, s), see text for details.



Transport equation for cosmic rays in the Galaxy

diffusion

energy loss (Bethe Bloch)

loss through interactions with ISM (spallation)

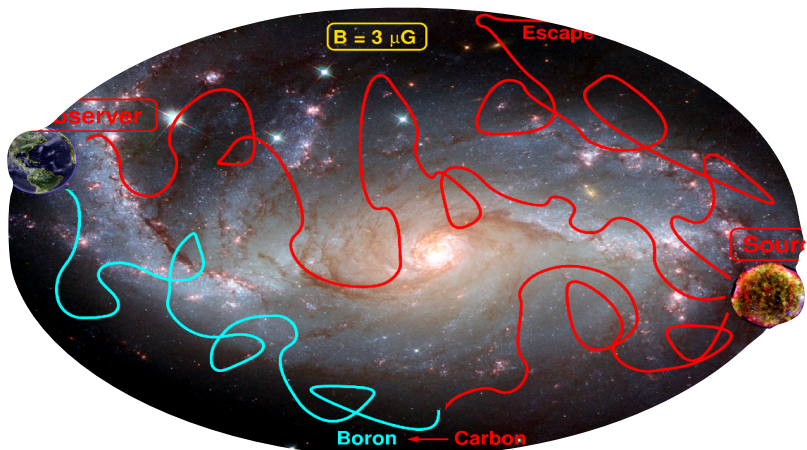
loss through radioactive decay

$$\frac{\partial N_i}{\partial t} = \nabla(D_i \nabla N_i) - \frac{\partial}{\partial E} (b_i N_i) - n\nu\sigma_i N_i - \frac{N_i}{\gamma\tau_i} + Q_i + \sum_{j>i} n\nu\sigma_{ij} N_j + \sum_{j>i} \frac{N_j}{\gamma_j\tau_{ij}}$$

source term

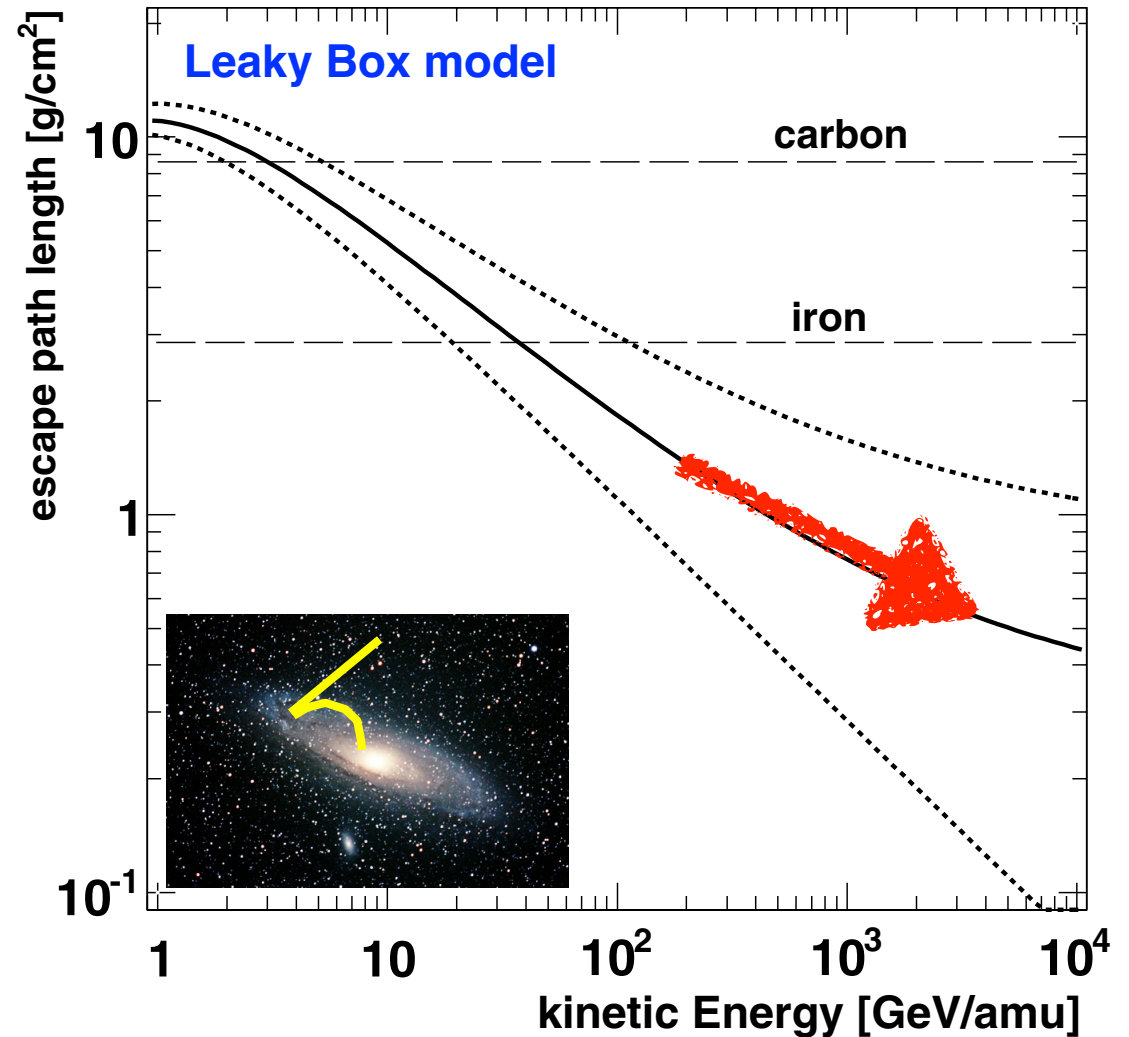
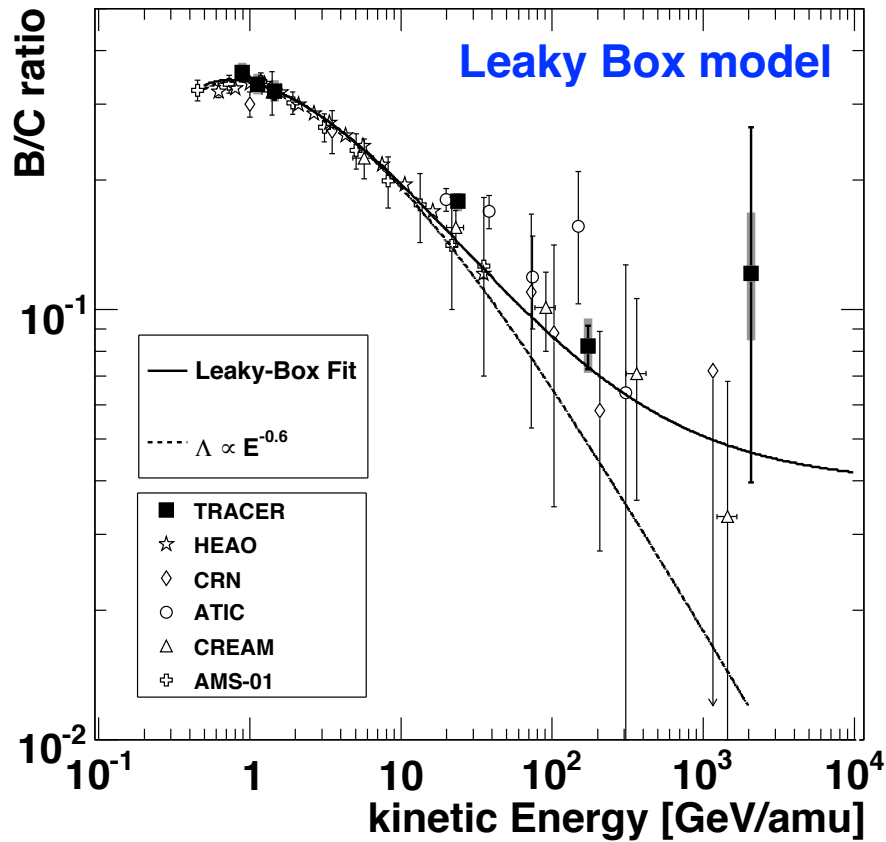
production through spallation of heavy nuclei

production through decay of heavy nuclei



Pathlength of cosmic rays in Galaxy

TRACER balloon experiment



Escape Path Length:

$$\Lambda_{esc}(E) = CE^{-\delta} + \Lambda_0$$

► Propagation index:

$$\delta = 0.64 \pm 0.02.$$

► Residual path length:

$$\Lambda_0 = 0.7 \pm 0.2 \text{ g/cm}^2.$$

$$\Lambda(R) = \frac{26.7\beta}{(\beta R)^\delta + (0.714 \cdot \beta R)^{-1.4}} + \Lambda_0 \text{ g/cm}^2,$$

Pathlength vs. interaction length

pathlength in Galaxy

$$\lambda_{esc} = 5 - 10 \text{ g/cm}^2$$

interaction length

nuclear radius

$$r = r_0 A^{1/3} \quad r_0 = 1.3 \cdot 10^{-13} \text{ cm}$$

cross section

$$\sigma_{p-A} = \pi (r_p + r_0 A^{1/3})^2$$

ISM: protons

$$n = 1/\text{cm}^3 \quad \rho = 1.67 \cdot 10^{-24} \text{ g/cm}^3$$

interaction length

$$\lambda_{p-A} = \frac{\rho}{\sigma_{p-A} \cdot n}$$

$$\lambda_{p-p} = 21 \text{ g/cm}^2 > \lambda_{esc}$$

$$\lambda_{p-Fe} = 1.6 \text{ g/cm}^2 < \lambda_{esc}$$

Shape of energy spectrum

$$\frac{dN}{dE} \propto E_0^\gamma$$

at source $\gamma \sim -2.1$

at Earth $\gamma \sim -2.6$ to -2.7

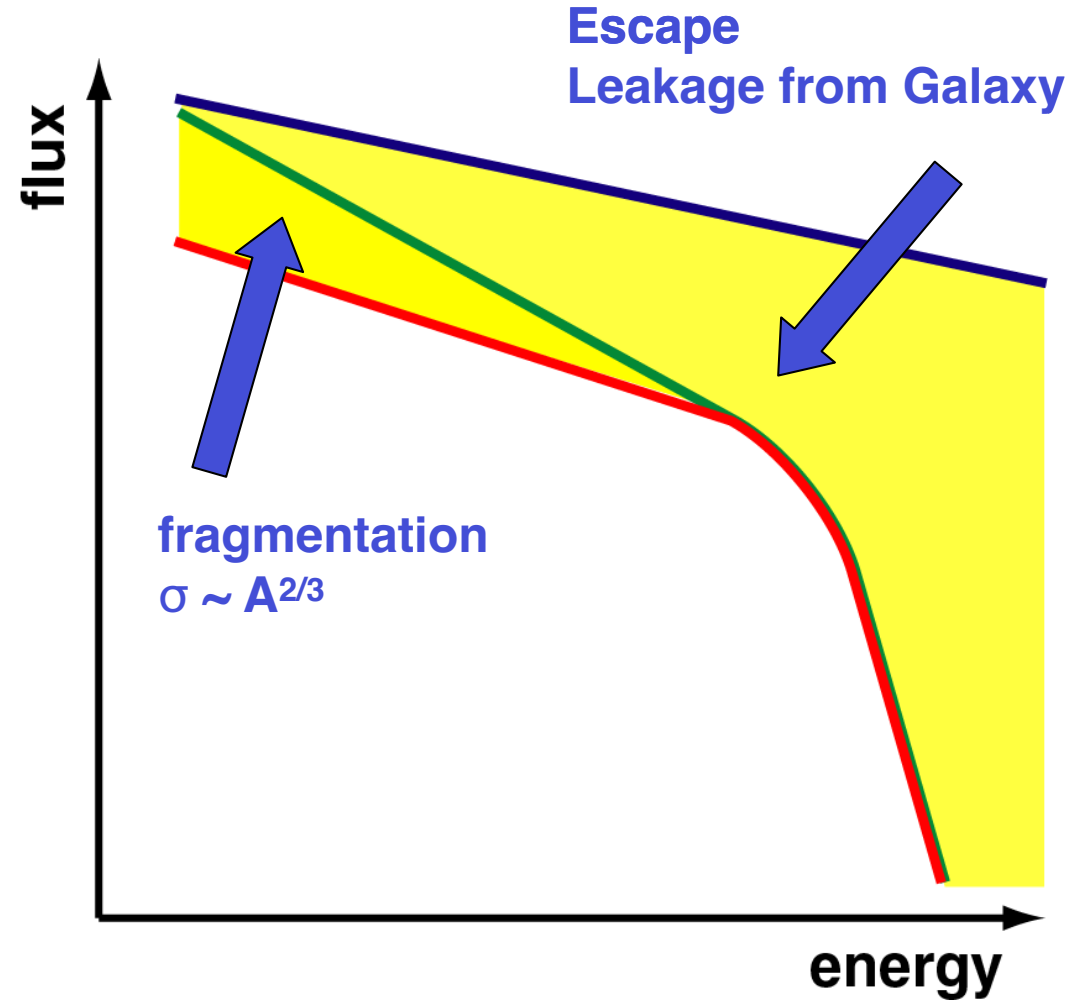
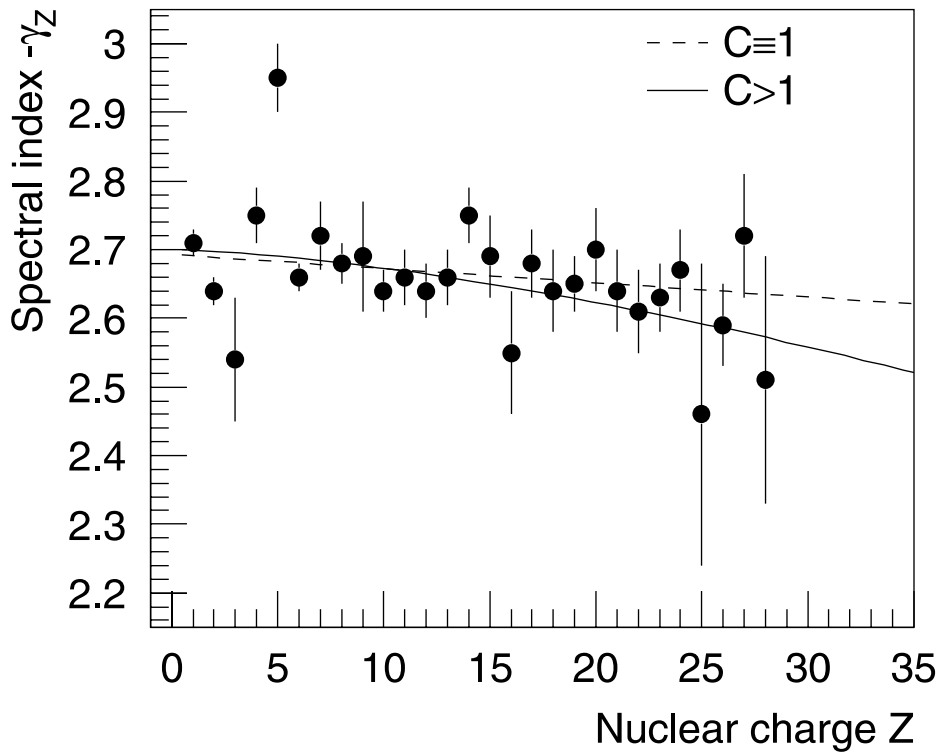


Fig. 5. Spectral index γ_Z versus nuclear charge Z (see Table 1). The solid line represents a three parameter fit according to Eq. (6), the dashed graph a linear fit.

Transport equation for cosmic rays in the Galaxy

diffusion

energy loss (Bethe Bloch)

loss through interactions with ISM (spallation)

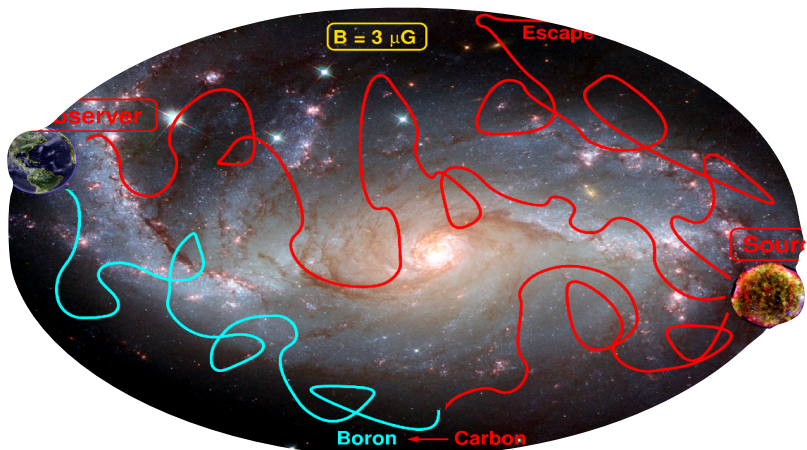
loss through radioactive decay

$$\frac{\partial N_i}{\partial t} = \nabla(D_i \nabla N_i) - \frac{\partial}{\partial E} (b_i N_i) - n v \sigma_i N_i - \frac{N_i}{\tau_i} + Q_i + \sum_{j>i} n v \sigma_{ij} N_j + \sum_{j>i} \frac{N_j}{\tau_{ij}}$$

source term

production through spallation of heavy nuclei

production through decay of heavy nuclei



Propagation of super-high-energy cosmic rays in the Galaxy

Jörg R. Hörandel ^{a,*}, Nikolai N. Kalmykov ^b, Aleksei V. Timokhin ^c

The steady-state diffusion equation for the cosmic-ray density $N(r)$ is (neglecting nuclear interactions and energy losses)

$$-\nabla_i D_{ij}(r) \nabla_j N(r) = Q(r). \quad (1)$$

$Q(r)$ is the cosmic-ray source term and $D_{ij}(r)$ the diffusion tensor.

Under the assumption of azimuthal symmetry and taking into account the predominance of the toroidal component of the magnetic field, Eq. (1) is presented in cylindrical coordinates as

$$\left[-\frac{1}{r} \frac{\partial}{\partial r} r D_{\perp} \frac{\partial}{\partial r} - \frac{\partial}{\partial z} D_{\perp} \frac{\partial}{\partial z} - \frac{\partial}{\partial z} D_A \frac{\partial}{\partial z} + \frac{1}{r} \frac{\partial}{\partial r} r D_A \frac{\partial}{\partial z} \right] N(r, z) = Q(r, z), \quad (2)$$

where $N(r, z)$ is the cosmic-ray density averaged over the large-scale fluctuations with a characteristic scale $L \sim 100$ pc [3]. $D_{\perp} \propto E^m$ is the diffusion coefficient, where m is much less than one ($m \approx 0.2$), and $D_A \propto E$ the Hall diffusion coefficient. The influence of Hall diffusion becomes predominant at high energies ($>10^{15}$ eV). The sharp

The magnetic field of the Galaxy consists of a large-scale regular and a chaotic, irregular component $\vec{B} = \vec{B}_{\text{reg}} + \vec{B}_{\text{irr}}$. A purely azimuthal magnetic field was assumed for the regular field

$$B_z = 0, \quad B_r = 0, \quad B_{\phi} = 1 \mu\text{G} \exp\left(-\frac{z^2}{z_0^2} - \frac{r^2}{r_0^2}\right),$$

where $z_0 = 5$ kpc and $r_0 = 10$ kpc are constants [3].

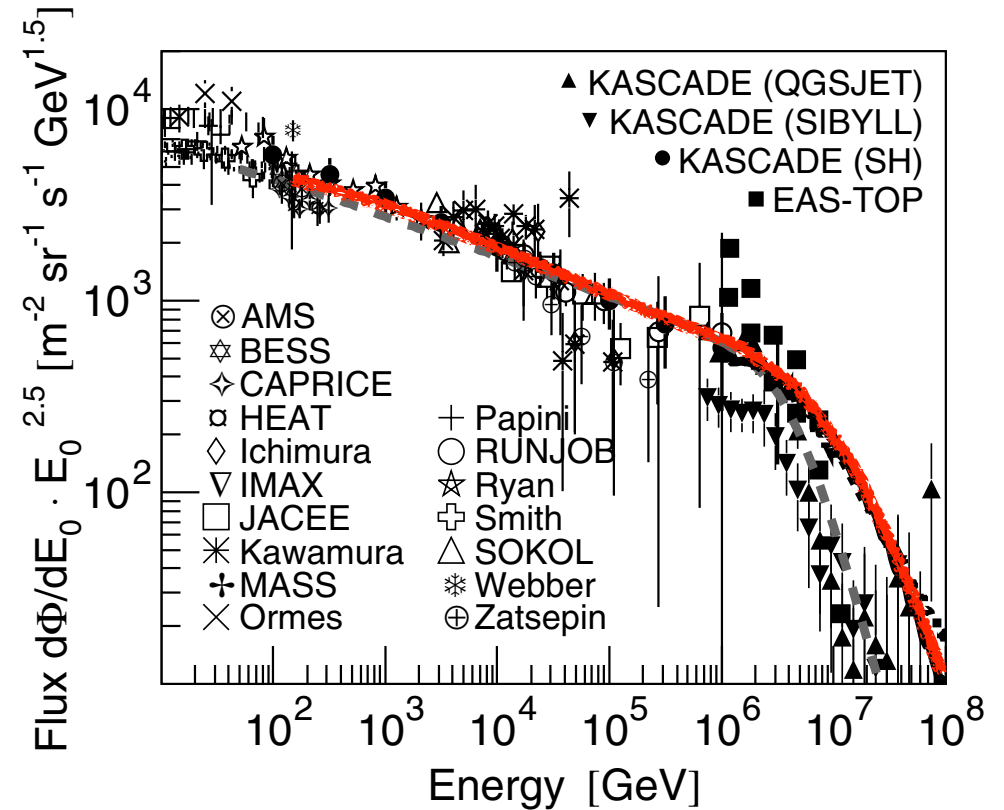
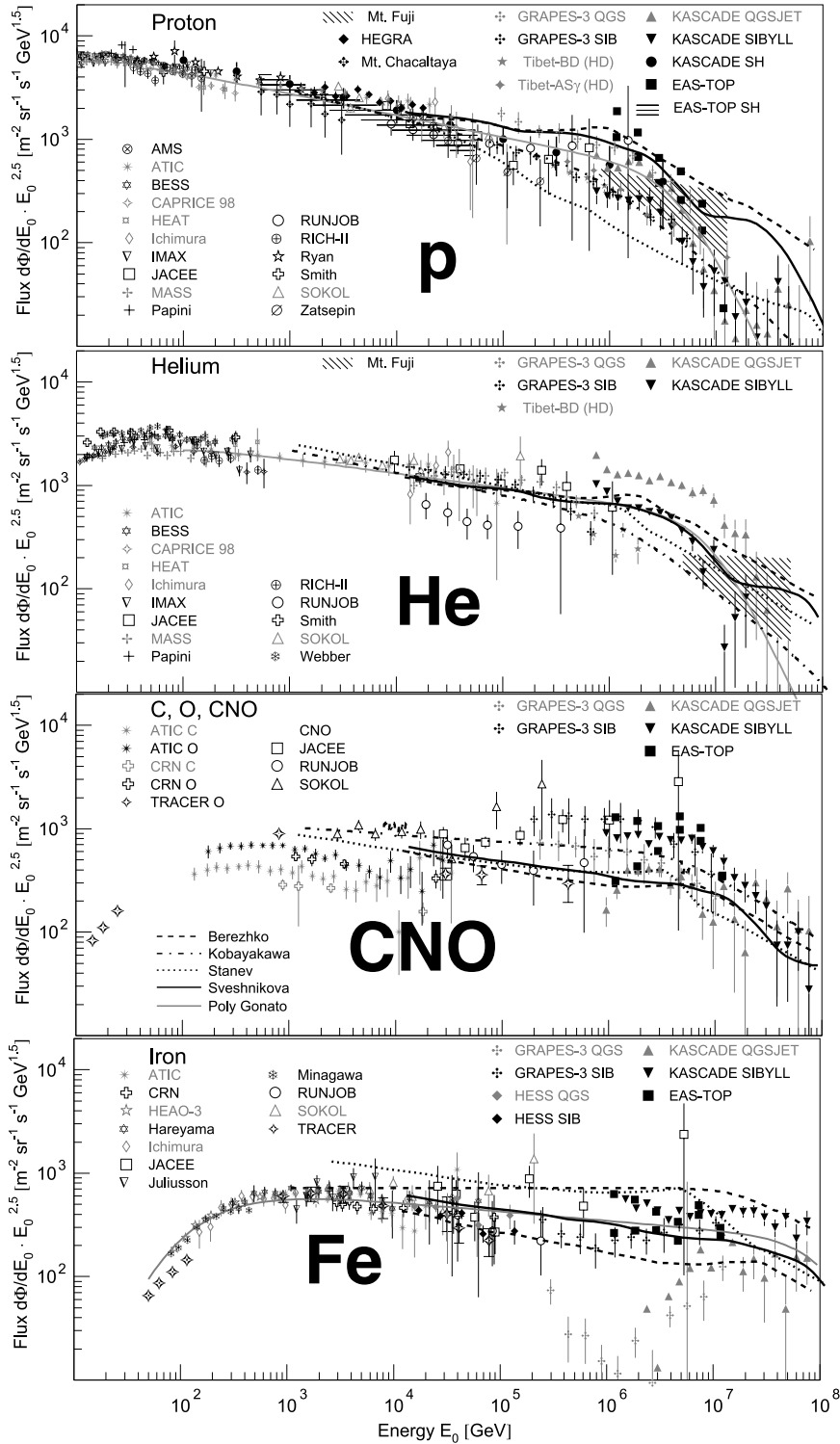


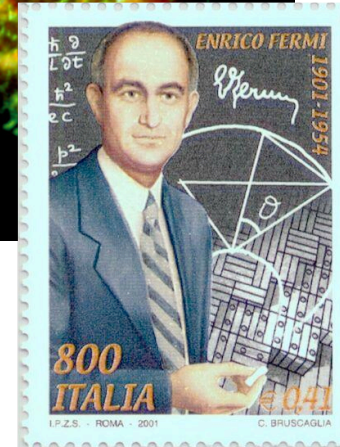
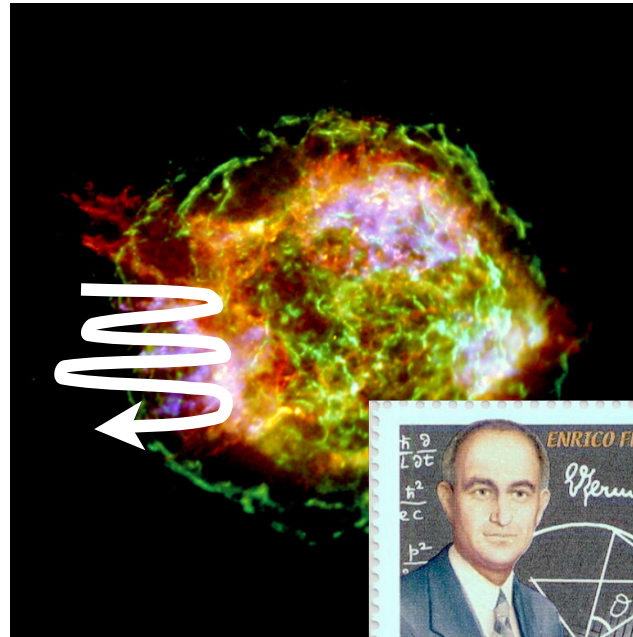
Fig. 7. Proton flux as obtained from various measurements, for references see [28], compared to the spectra shown in Fig. 6 (black lines) and the *polygonato* model [26] (grey, dashed line).

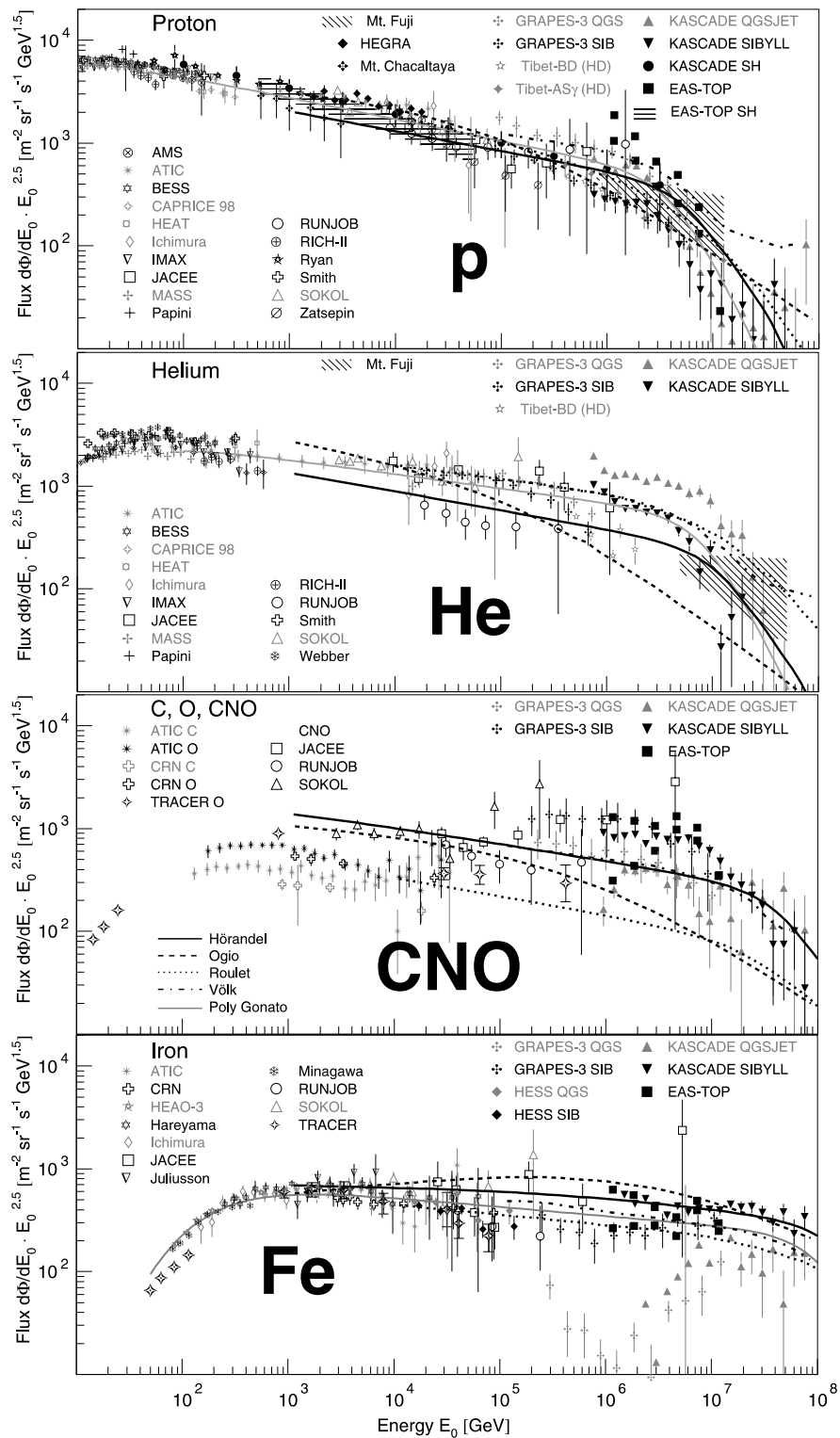


maximum energy

$$E_{max} \propto B \cdot Z$$

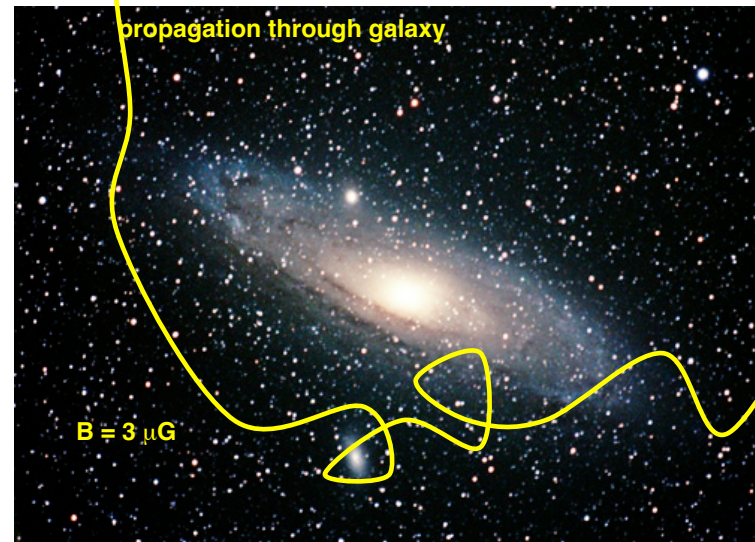
$$E_{max} \approx Z \cdot 100 \text{ TeV} \dots Z \cdot 5 \text{ PeV}$$





leakage from Galaxy

$$E_k \propto Z$$



Transition to extragalactic CR component

J. Blümer et al. / Progress in Particle and Nuclear Physics 63 (2009) 293–338

327

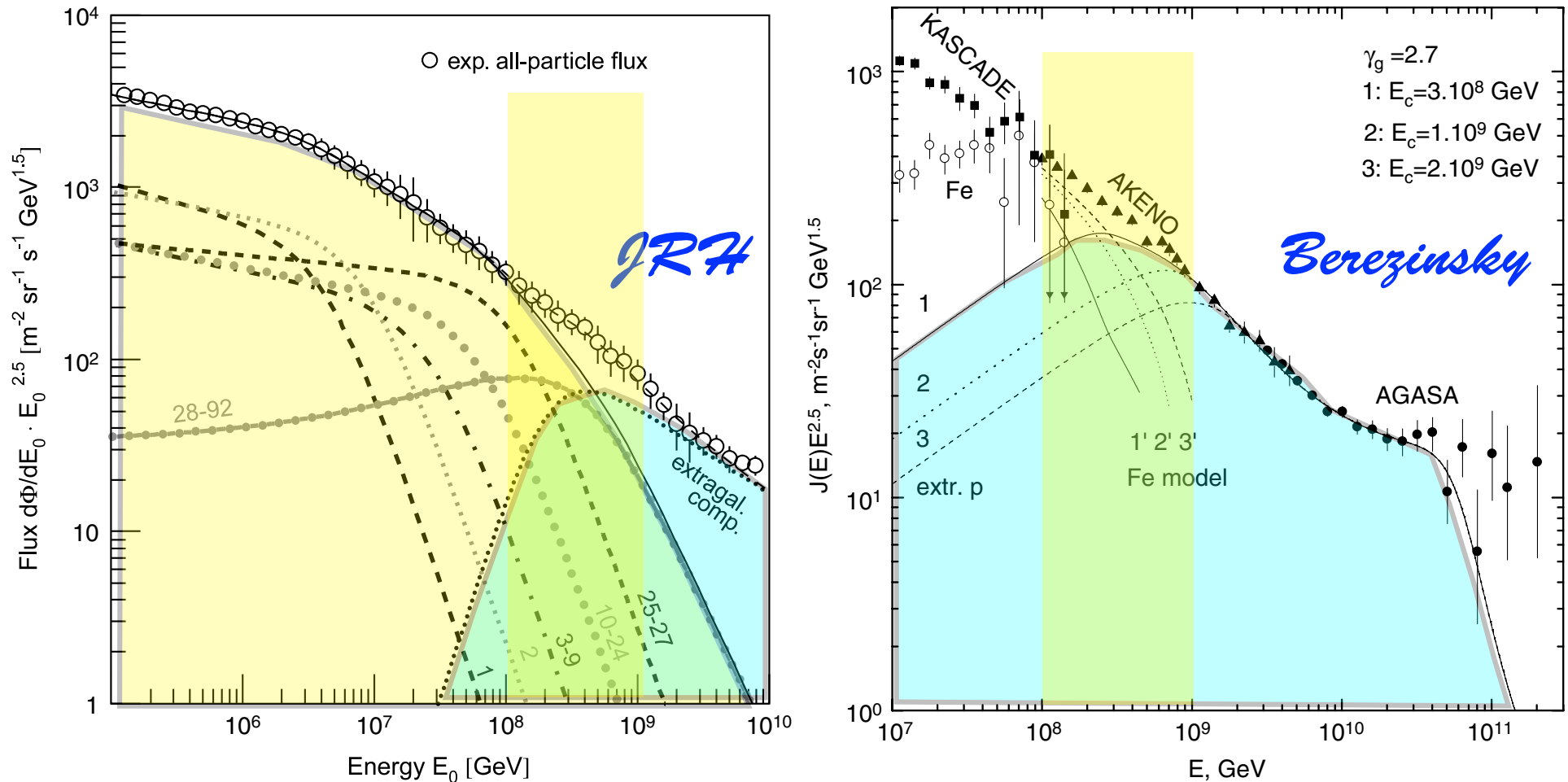
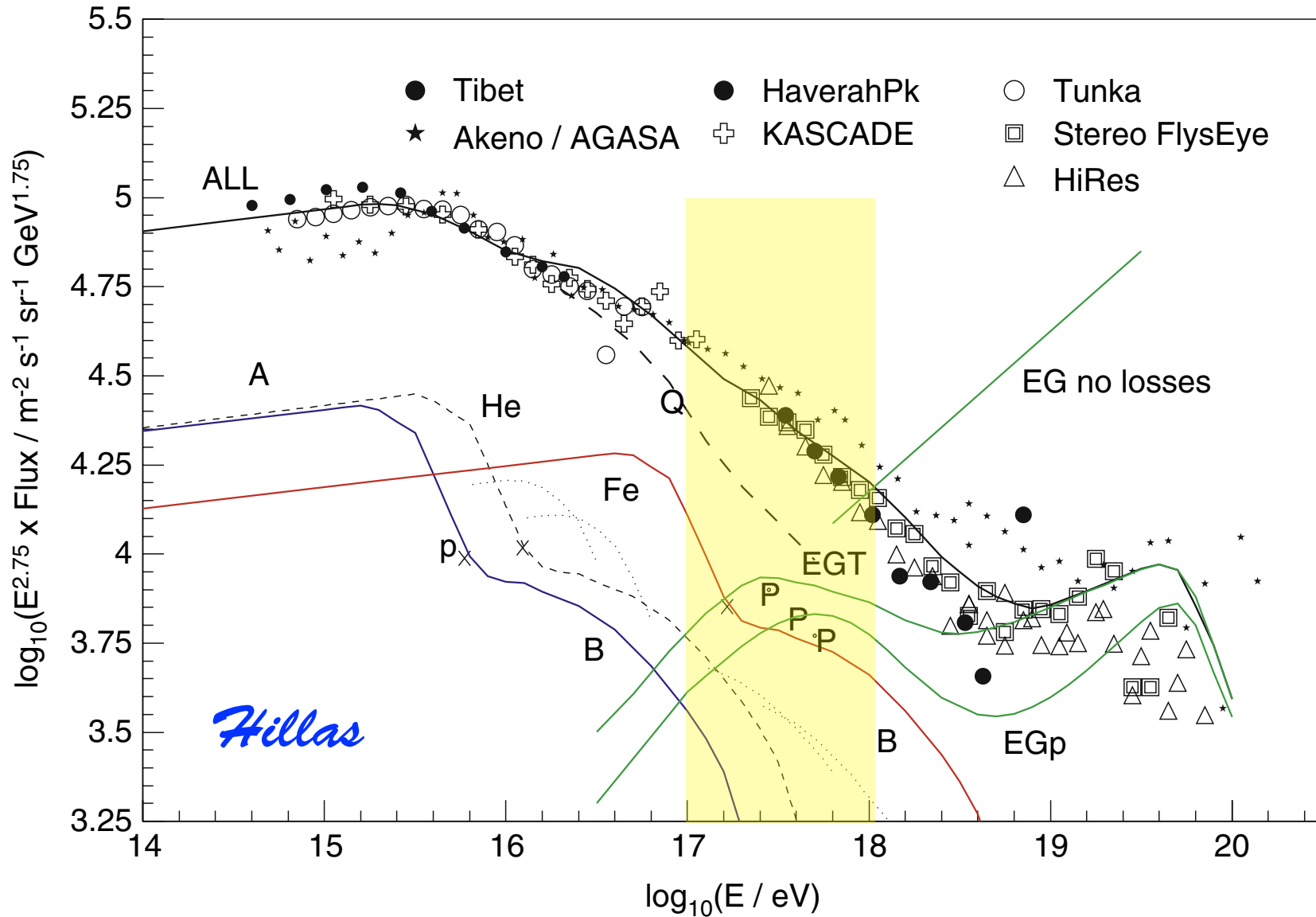


Fig. 26. *Left panel:* Cosmic-ray energy spectra according to the poly-gonato model [2]. The spectra for groups of elements are labeled by their respective nuclear charge numbers. The sum of all elements yields the galactic all-particle spectrum (—) which is compared to the average measured flux. In addition, a hypothetical extragalactic component is shown to account for the observed all-particle flux (- - -). *Right panel:* Transition from galactic to extragalactic cosmic rays according to Berezhinsky et al. [451]. Calculated spectra of extragalactic protons (curves 1, 2, 3) and of galactic iron nuclei (curves 1', 2', 3') are compared with the all-particle spectrum from the Akeno and AGASA experiments. KASCADE data are shown as filled squares for the all-particle flux and as open circles for the flux of iron nuclei.

Transition to extragalactic CR component



„classical“ supernovae + additional component

Contribution of (regular) SNR-CR to all-particle spectrum

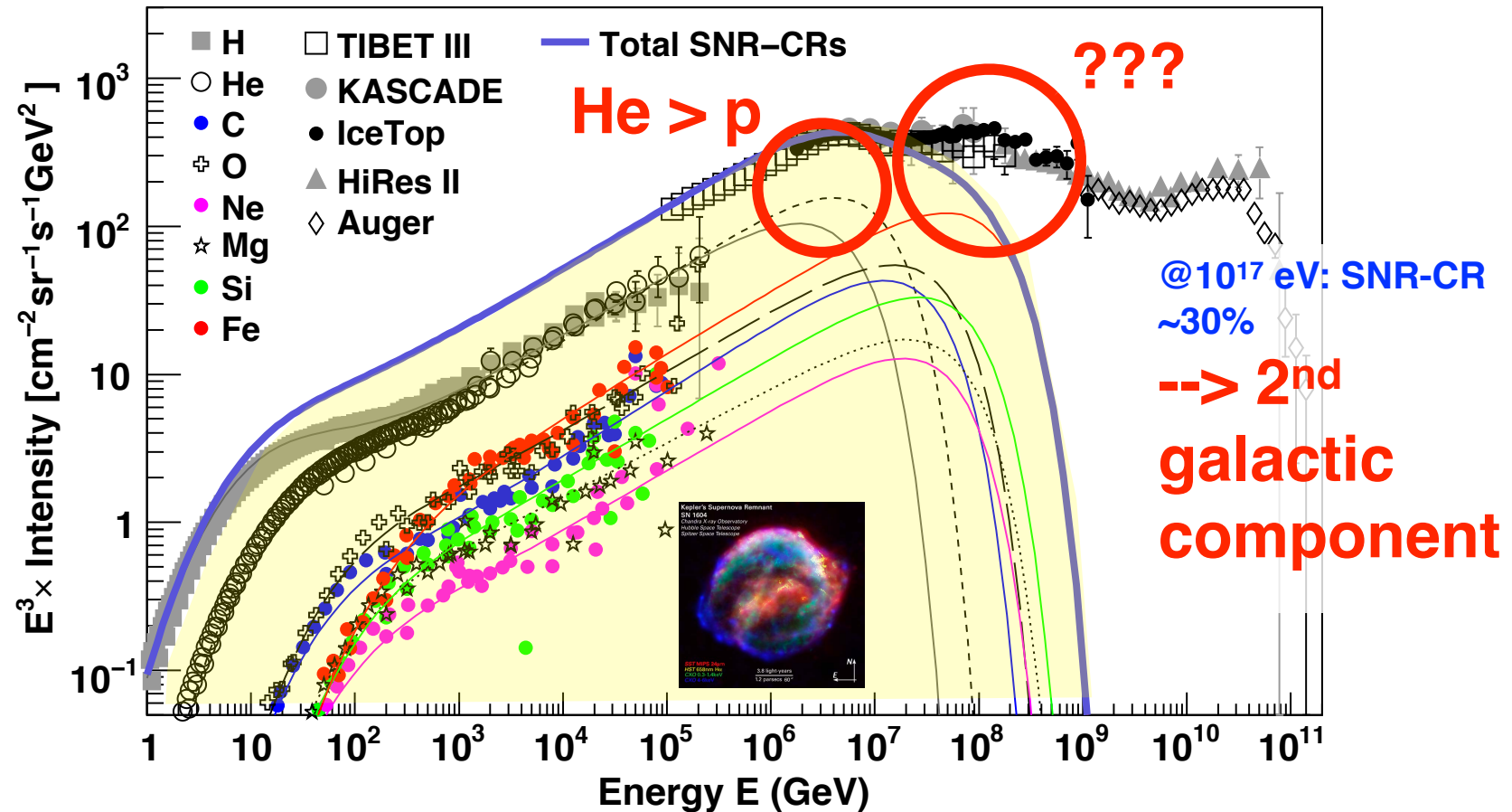
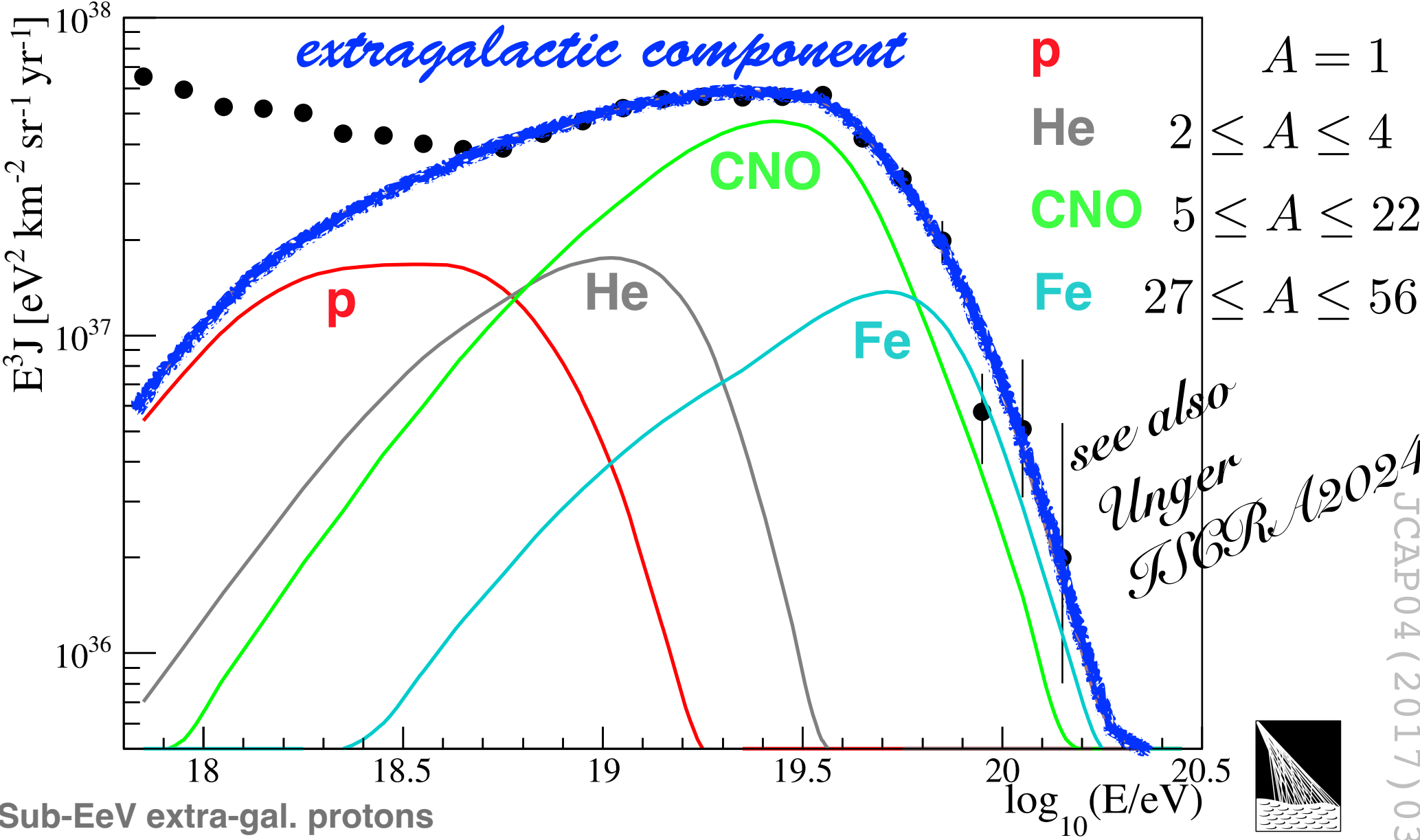


Fig. 2. Contribution of SNR-CRs to the all-particle cosmic-ray spectrum. The thin lines represent spectra for the individual elements, and the thick-solid line represents the total contribution. The calculation assumes an exponential cut-off energy for protons at $E_c = 4.5 \times 10^6$ GeV. Other model parameters, and the low-energy data are the same as in Figure 1. Error bars are shown only for the proton and helium data. High-energy data: KASCADE (Antoni et al. 2005), IceTop (Aartsen et al. 2013), Tibet III (Amenomori et al. 2008), the Pierre Auger Observatory (Schulz et al. 2013), and HiRes II (Abbasi et al. 2009).

~8% of mechanical power of SN --> CRs

Combined fit of spectrum and composition data as measured by the Pierre Auger Observatory



Sub-EeV extra-gal. protons from interactions of heavier nuclei

see also Unger JSOR A2024



JCAP04(2017)038

all-particle spectra including 2nd galactic component

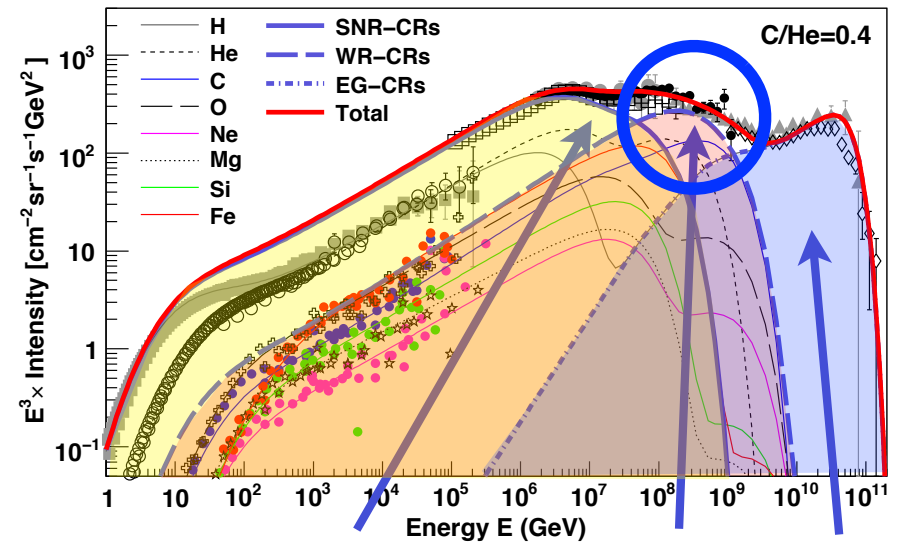
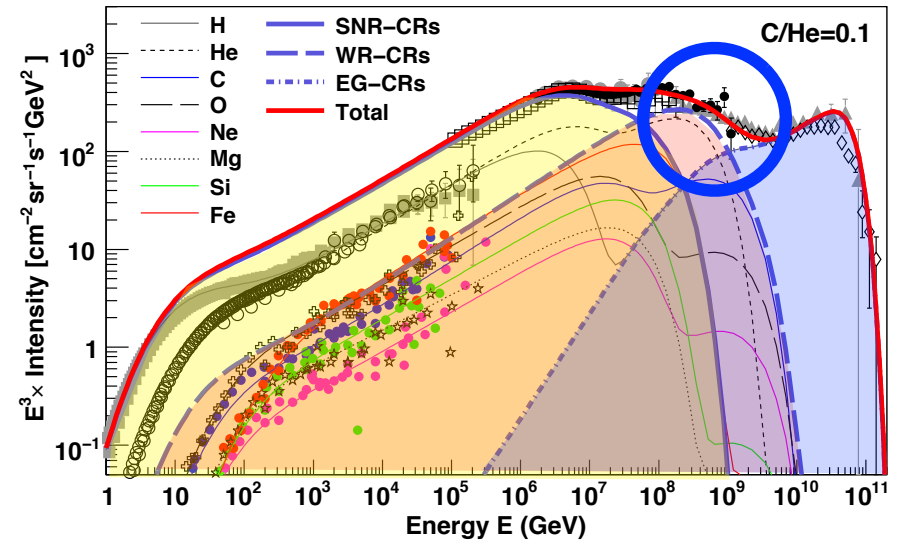
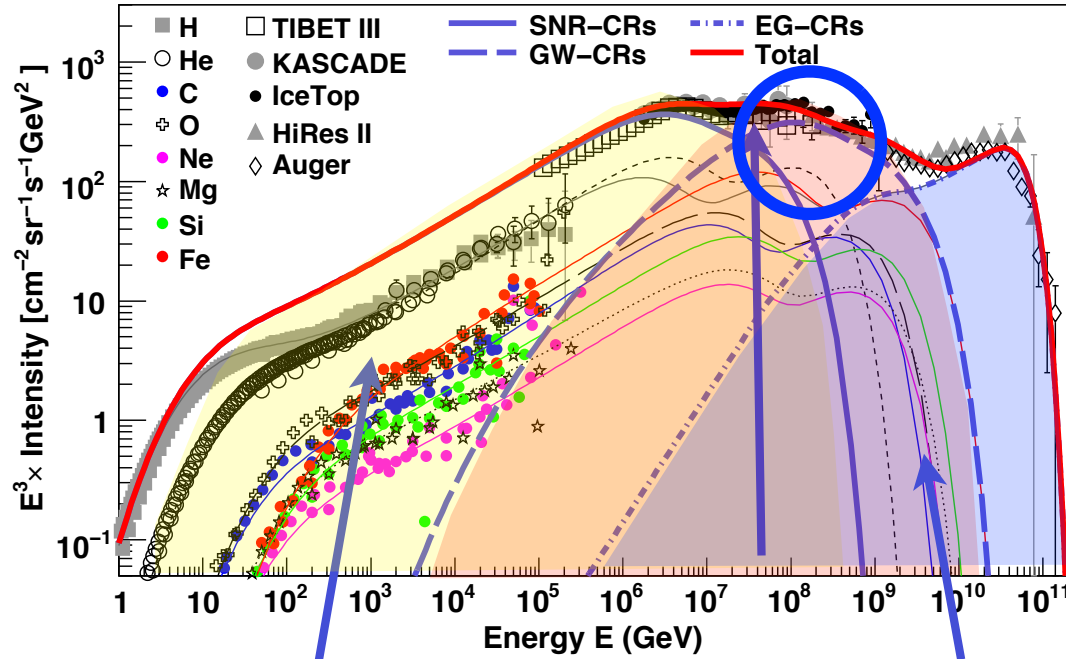


Table 3. Injection energy of SNR-CRs used in the calculation of all-particle spectrum in the WR-CR model (Figure 6).

Particle type	C/He = 0.1 $f(\times 10^{49} \text{ ergs})$	C/He = 0.4 $f(\times 10^{49} \text{ ergs})$
Proton	8.11	8.11
Helium	0.67	0.78
Carbon	2.11×10^{-2}	0.73×10^{-2}
Oxygen	2.94×10^{-2}	2.94×10^{-2}
Neon	4.41×10^{-3}	4.41×10^{-3}
Magnesium	6.03×10^{-3}	6.03×10^{-3}
Silicon	5.84×10^{-3}	5.84×10^{-3}
Iron	5.77×10^{-3}	5.77×10^{-3}

S. Thoudam et al., A&A 595 (2016) A33

Cosmic rays at the knee

Results and implications

- knee in all-particle spectrum at ~ 4.5 PeV caused by fall-off of light elements (p, He)
- experimental (world) data indicate rigidity-dependent fall-off of individual elements
(in particular unfolding by KASCADE[-Grande] and IceCube/Top)
- spectrum above knee is superposition of individual spectra (elemental knees)
 - > fine structure in all-particle spectrum
 - > end of galactic CR component
- astrophysical origin of knee:
combination of maximum energy attained in sources (Supernovae) (Hillas criterion)
and leakage from Galaxy
- 2nd galactic component at $\sim 10^{17}$ eV?
- extra-galactic origin $> 10^{18}$ eV



Nikhef

